Geochemical evidence for the nonexistence of supercritical geothermal fluids at the Yangbajing geothermal field, southern Tibet

Yingchun Wang[a,b] Liang Li[a,c] Huaguo Wen[a,c,*] Yinlei Hao[d]

a State Key Laboratory of Oil and Gas Reservoir Geology and Exploitation, Chengdu University of Technology, Chengdu 610059, China

b College of Energy Resources, Chengdu University of Technology, Chengdu 610059, China

c Institute of Sedimentary Geology, Chengdu University of Technology, Chengdu 610059, China

d School of Environmental Science and Engineering, Southern University of Science and Technology, Shenzhen 518055, China

Highlights

The thermal decomposition of marine carbonates and metasediments is a source of CO_2.

The radioactive decay of U and Th within crustal granite is the dominant source of He.

Three thermal reservoirs were identified using multiple gas geothermometers.

The parent geothermal fluid had a temperature of ∼320 °C at an ∼8-km depth.

Yangbajing has no supercritical fluids, given its small, deep-seated magma chamber.

Abstract

Exploring and exploiting high-temperature (even supercritical) geothermal resources are significant to meet energy demands and reduce carbon emissions. The Yangbajing geothermal field is the most exploited in China, with the currently highest temperature (329.8 °C) measured in a geothermal well. However, whether there are supercritical geothermal fluids beneath the deep parts of this geothermal field is under controversy. In this paper, the water isotope, chemical compositions, and C–He isotopes of gas samples were collected and analyzed. The geothermal water originated from the mixing of meteoric water and magmatic water (25%). The sources of CO2 in the geothermal field were dominated by the thermogenic degassing of carbonates and metasediments in the crust while the radioactive decay of U and Th in granite is the dominated source of He. The temperatures of three different reservoirs are 150 ± 15 °C, 250 ± 10 °C, and ∼320 °C (with a depth of ∼8 km), respectively. These were obtained using dissolved gas, soil CO2 flux, and noble gas geothermometers. Unlike other supercritical geothermal fields worldwide with larger, shallower, basaltic magma chambers, the Yangbajing geothermal field has a deep-seated, small-scale, granitic magma chamber. Thus, its geological conditions are not conducive for gestating supercritical fluids. These results are of great significance for exploring and developing high-temperature (even ultra-high-temperature) geothermal resources in China.

Keywords

Gas geothermometer; Geothermal fluid; Reservoir temperature; Supercritical geothermal fluids; Yangbajing geothermal field

1. Introduction

Clean and renewable energy sources are increasingly becoming important in response to global climate change. Among these, geothermal energy contributes more and more to reducing environmental pollution and increasing the proportion of renewable energy (Karlsdottir et al., 2020). Earth's heat energy is immense—over 99% of the Earth has temperatures exceeding 1000 ℃ (Chambefort and Stefánsson, 2020). Thus, the exploration and exploitation of geothermal energy, particularly high-temperature and supercritical (T > 374 ℃, P > 22 MPa) geothermal resources (Reinsch et al., 2017, Feng et al., 2021), have become essential in strategically planning energy consumption for all countries around the world.

Most of the high-temperature geothermal systems in China are located in Tibet, Yunnan, and Sichuan provinces, forming part of the Himalayan geothermal belt (Liao, 2018). The Yangbajing geothermal field in southern Tibet, China, is the earliest explored and developed high-temperature geothermal field in China (Dor, 2003, Guo et al., 2007). It has been continuously studied for more than 40 years, and its current installed capacity has reached 25.18 MW (Zhang et al., 2019). A steady-state temperature measurement of its borehole ZK4002 was conducted in 1994 and the measured temperature was 329.8 ℃ at a depth of about 1500 m, which is currently the highest measured temperature in a geothermal well in China (Fan, 2002, Guo et al., 2007). After years of research, the characteristics and properties of the fluid sources (Guo et al., 2007, Guo, 2012, Yuan et al., 2014), heat source (Brown et al., 1996, Nelson et al., 1996, Wei et al., 2001), and fluid channels and reservoir (Zhao et al., 2011, Feng et al., 2012) of the Yangbajing geothermal field have been studied systematically on varying degrees from the perspectives of geology, fluid geochemistry, geophysics, and altered minerals (Makovsky and Klemperer, 1999, Dor, 2003, Wang et al., 2018). Thus, a relatively consistent knowledge of the geothermal field has been formed.

The circulation of the thermal groundwater of the Yangbajing geothermal field is driven by the huge terrain elevation difference. The thermal groundwater is currently estimated to exceed a 5 km depth, where it is speculated to have reached the brittle-ductile transition zone (Su et al., 2020). As previously mentioned, the geothermal fluid temperature exceeds 300 ℃ at a depth of 1.5 km. If it reaches a depth of 5 km, the temperature would exceed 400 ℃ according to the geothermal gradient (40 ℃/km) (Kang et al., 1985, Zhao et al., 2011) and form supercritical geothermal fluids. This raises the question of whether there are supercritical geothermal fluids in the deep part (>5 km) of the Yangbajing geothermal field. Analyzing the gas characteristics of the geothermal field and estimating the temperature of the reservoir are the most economical and convenient ways to answer this question. Gases are the bridge between the deep structures and energy characteristics and the surface thermal manifestations of a geothermal field. The chemistry and the isotopes of gases play an important role in geothermal exploration and development (Arnórsson, 2000). For example, geothermal gas and isotopic characteristics can reveal the heat source properties (Karakuş, 2015, Tian et al., 2018, Pan et al., 2021) and reflect the geodynamic mechanisms (Ciotoli et al., 2016) of geothermal fields during the geothermal exploration stage. Changes in geothermal gas characteristics over time can reveal the responses of thermal reservoirs during geothermal energy development and

utilization, providing meaningful guidance for the sustainable use of geothermal resources (Caracausi et al., 2005, Monterrosa and Montalvo López, 2010, Tassi et al., 2014). Through the research and analysis of geothermal gas and isotopic characteristics, identifying the source of the fluid composition of the geothermal field and the geochemical processes that the fluid experienced (such as magma degassing and mixing) is possible (Fan et al., 2019; Tian et al., 2019; Hao et al., 2020b). Moreover, some abnormal gas components such as hydrogen and helium are also important associated resources (Hao et al., 2020a).

Geothermal gases can also be used in estimating the temperature through the thermodynamic equilibrium process of geothermal gases in a reservoir. Sets of gas geothermometers based on the concentration of reactive gases have been used to investigate the subsurface temperatures of geothermal systems. These include some single gas thermometers such as CO_2, H_2S, or H_2 (Arnórsson and Gunnlaugsson, 1985) and those with two or more gases such as CO_2–H_2, H_2S–H_2, and H_2O–H_2–CO_2–CO–CH_4 (Chiodini and Marini, 1998, Fiebig et al., 2004). These may also be based on gas ratios such as CO_2/Ar, H_2/Ar, and CO_2/N_2 (Arnórsson, 2000). Notably, the estimated temperatures based on gas–gas relationships and gas–mineral equilibria in reservoirs and the gas content and ratio in the geothermal fluid are quenched as these fluids ascend to the surface (Giggenbach, 1980, Arnórsson, 2000). Thus, these reactive gases are sensitive to the exiting processes (e.g., steam condensation and boiling) of fluids as they ascending to the surface. Even so, they have been used in many cases and still give appropriate reservoir temperatures (Karolytė et al., 2019). However, these inherent processes limit the use of gas geothermometers and make it hard to determine reservoir conditions and secondary processes (Stefánsson, 2017). Moreover, reservoir temperatures obtained by assuming a gas–gas or gas–mineral equilibrium are not always acceptable (Lowenstern et al., 2015, Karolytė et al., 2017). Fortunately, the development of some gas geothermometers in recent years (Harvey et al., 2017, Byrne et al., 2021) has provided new opportunities for reservoir temperature estimation with advanced experimental technologies, which may be useful in detecting supercritical geothermal systems.

Most supercritical geothermal systems are related to magma chambers at depths of 2–6 km (Scott et al., 2015, Stimac et al., 2015, Jolie et al., 2021). Significant and focused heat transfer typically occurs between the upside of magma chambers and the bottom of production wells. This part is almost at the root of conventional geothermal systems (Scott et al., 2017), with the most favorable conditions for high-enthalpy and supercritical geothermal systems (Scott et al., 2016) and major types of ore deposits (Heinrich and Candela, 2014). Several supercritical geothermal systems have been observed around the world, including those at the Salton Sea, The Geysers, and Hawaii, USA (Garcia et al., 2016, Kaspereit et al., 2016); Kakkonda, Japan (Muraoka et al., 1998); Larderello, Italy (Minetto et al., 2020); Reykjanes, Krafla, and Nesjavellir, Iceland (Friðleifsson et al., 2017, Reinsch et al., 2017); Los Humeros, Mexico (Peiffer et al., 2018); and Menengai, Kenya (O'Sullivan et al., 2015). In this regard, supercritical fluids are related to the circulation of infiltrated meteoric water around magma intrusions (Hayba and Ingebritsen, 1997, Scott et al., 2016). Their primary components are CO_2, H_2S, and other acid gases due to the magma degassing (Henley and Seward, 2018, Heřmanská et al., 2020). They may result from chemical and physical processes, such as phase segregation, conductive heating of groundwater near an intrusion,

magma degassing, or condensation of liquids (Heřmanská et al., 2019). The host rock permeability, the emplacement depth and geometry of an intrusion, the temperature-dependent permeability near an intrusion, and the depth and extent of boiling zones are the key geological controls affecting supercritical fluids (Scott et al., 2016). Boiling zones are located within 1 km above intrusions at depths of 3–4 km with permeabilities of $>10^{-15}$ m^2. These boiling areas get smaller with deeper intrusions and lower permeabilities (Scott et al., 2017). The permeability may decrease to 10^{-20} m^2 at a depth of 10 km, making it impossible for supercritical geothermal fluids to form (Wanner et al., 2020).

In this paper, we collected geothermal fluids samples from hot springs and geothermal wells and compiled the historical data of the Yangbajing geothermal field. We wanted to determine whether there are supercritical geothermal fluids in Yangbajing using fluid chemistry and isotope evidence. The geochemical characteristics of the geothermal fluids were analyzed, and the reservoir temperatures of the geothermal field were re-evaluated using several new geothermometers. The results are significant for the exploration and development of high-temperature and ultra-high-temperature geothermal resources around China and for the in-depth understanding of the geodynamic processes of the Yadong–Gulu rift zone.

2. Geological setting of the Yangbajing geothermal field

The Yangbajing geothermal field is located in the hinterland of the Qinghai–Tibet Plateau, 90 km northwest of Lhasa (Fig. 1). This geothermal field has the largest installed capacity for geothermal power and provided 60% of Lhasa's electricity supply in the 1990s (Dor, 2003). The geothermal wells and numerous thermal springs in this geothermal field cover an area of approximately 40 km^2. The annual average temperature in Yangbajing is 2.5 ℃, and the highest and lowest recorded air temperatures are 23.4 ℃ and −25.7 ° C, respectively. The average annual rainfall in Yangbajing is 383 mm, and 65% of which is concentrated from July to August (Guo et al., 2007).

The Yangbajing geothermal field is located in the middle part of the famous Yadong–Gulu rift system. To the northwest are the Nyainqentanglha Mountains, and to the southeast are the Tang Mountains (Fig. 1b). The basement of the geothermal system comprises Carboniferous–Permian slate, Upper Cretaceous carbonate, and Jurassic metasediments in the southeast, with Paleozoic gneiss and migmatite in the northwest (Dor, 2003, Wang et al., 2014). The magmatic rock around the geothermal field includes the Late Yanshanian–Himalayan granite, with a K–Ar radiometric age of 8.1 Ma (Fig. 2a) (Zhao et al., 2003). However, no Quaternary volcanic activity has been found in the Yangbajing area so far, and partial melting at depths of 15–20 km is speculated as the heat source of the geothermal system (Teng et al., 2019) based on the observed "bright spots" from the INDEPTH (International Deep Profiling of Tibet and the Himalaya) project (Brown et al., 1996, Chen et al., 1996, Kind et al., 1996, Makovsky et al., 1996, Nelson et al., 1996). Two sets of normal faults striking NNE and NE are respectively distributed on the east and west sides of the faulted basin. These extensional faults are inferred as flow channels for

the storage and migration of geothermal fluids as they continued to be active until the late Quaternary (Fig. 3) (Guo et al., 2007). The Yangbajing area has strong surface thermal manifestations, including boiling springs, hot springs, hydrothermal explosions, steaming grounds, and sinters deposited before the geothermal power plant was constructed in 1981 (Tong et al., 2000). However, some of these hydrothermal activities have disappeared as the geothermal exploration continues (Liao, 2018). The current electric power generated at the geothermal field mainly depends on the geothermal fluids from the shallow reservoir, whereas less than one-fifth is from the deep reservoir (Guo et al., 2007).
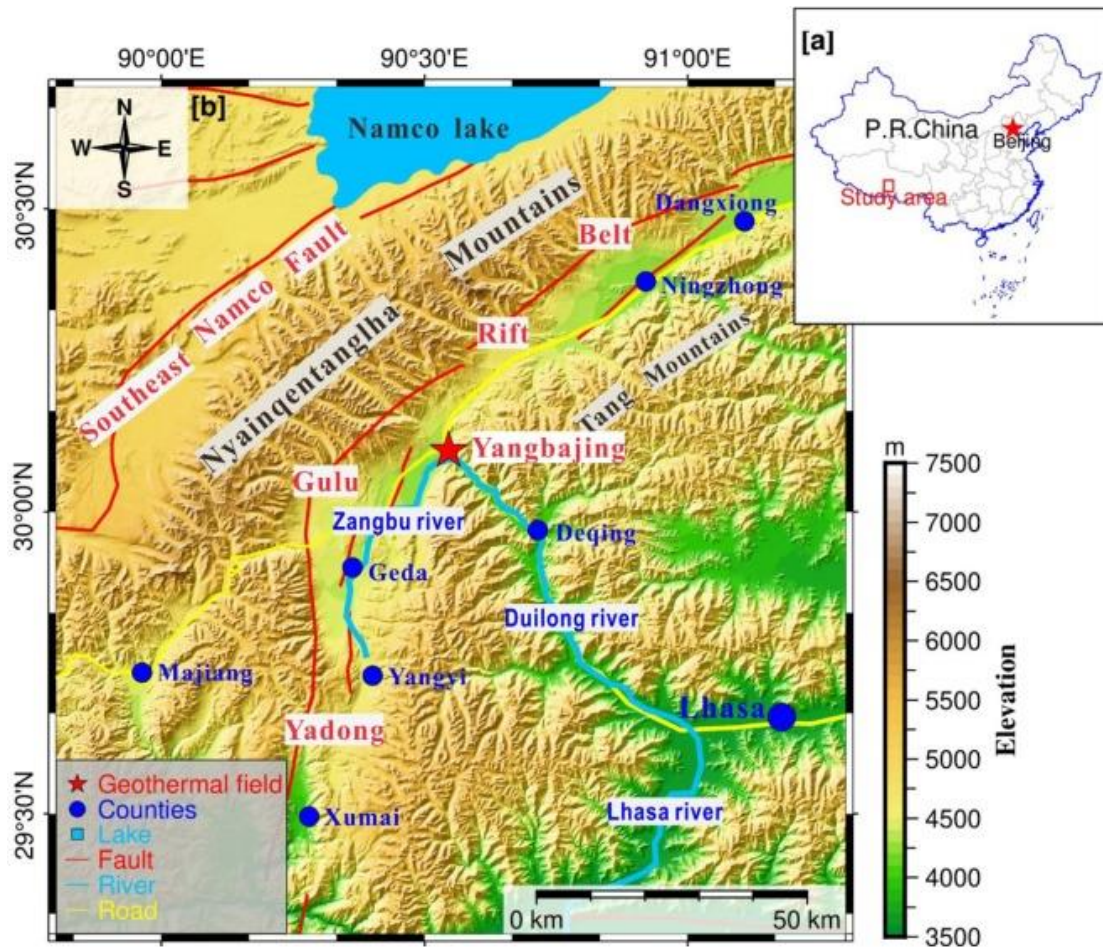

Fig. 1. The topography and tectonic location of the Yangbajing geothermal field.

The precipitation and snowmelt from the Nyainqentanglha Mountains (with an elevation between 4500 and 5800 m) are the primary recharge source of the geothermal field in the northwest (Guo, 2012, Tan et al., 2014). Meteoric water infiltrates to a certain depth and is heated by the host rock. Thermal fluids rise into the deep reservoir along the fault belt and then flow into the shallow thermal reservoir, where they mix with cold groundwater and flow to the southeast part of the field together (Fig. 3) (Guo, 2012).

There are two distinct reservoirs under the Yangbajing geothermal field: the deeper one is at a depth of 950–1850 m, whereas the shallower reservoir is at 300–500 m (Dor, 2003, Guo, 2012). The temperature of the deep reservoir is about 250 ℃, according to the data from the borehole ZK4001. In contrast, the temperature of the shallow reservoir is between 130 ℃ and 170 ℃ (Guo, 2012). The petrography of the shallow reservoir is mainly

weathered granite and Quaternary sandstones in the northwestern part of the geothermal field and Himalayan granite overlain by Quaternary sediments and underlain by boulder clay and silty clay in the southeastern part (Fig. 3) (Guo et al., 2007). The deep reservoir comprises fissure granitic mylonite, biotite granite, and fissure granites covered with strongly weathered granites, which have low permeability as the initial feldspar has been altered to kaolinite. The plastic shear zone consists of granitic mylonite toward the southeast, with a dip of 30 °cutting the granite bedrock. The high-angle normal faults in front of the Nyainqentanglha Mountains extend to a depth of more than 5 km, cutting the granitic mylonite and forming deep thermal reservoirs along with these fragments (Fig. 3) (Guo et al., 2007).
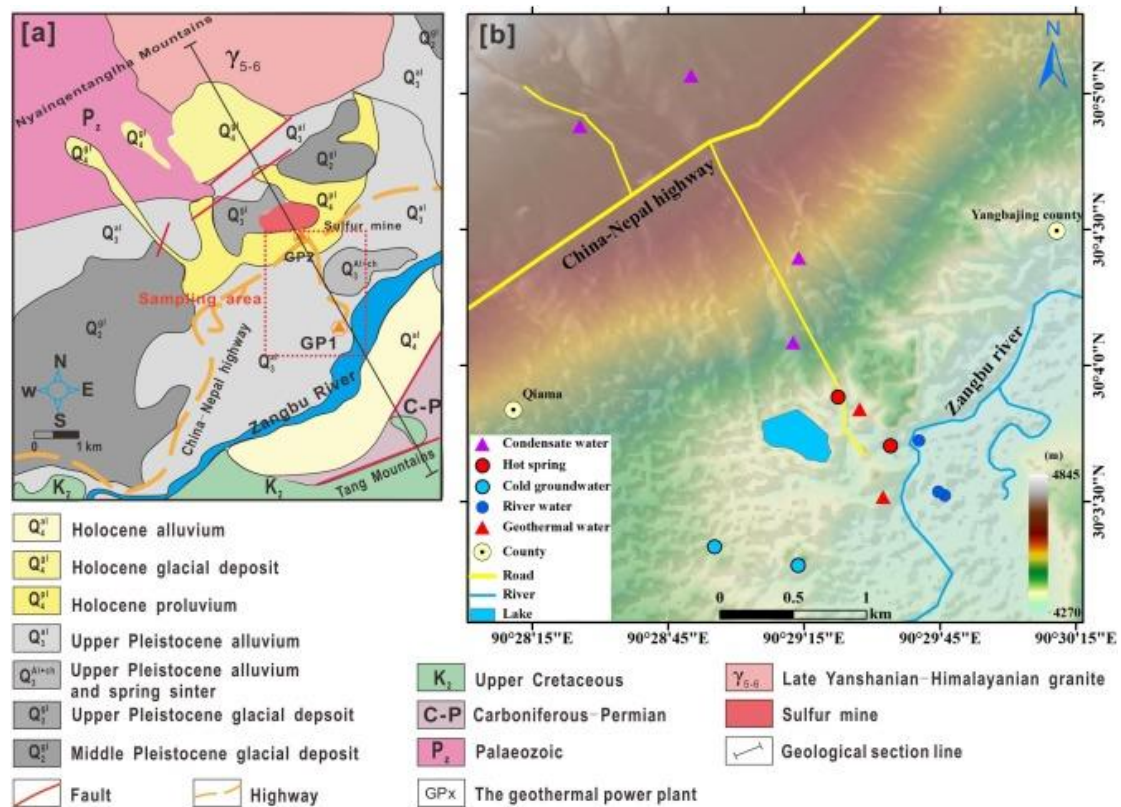

Fig. 2. (a) Geological map (modified from Guo et al., 2007) and (b) Distribution of sample points in the Yangbajing geothermal field.
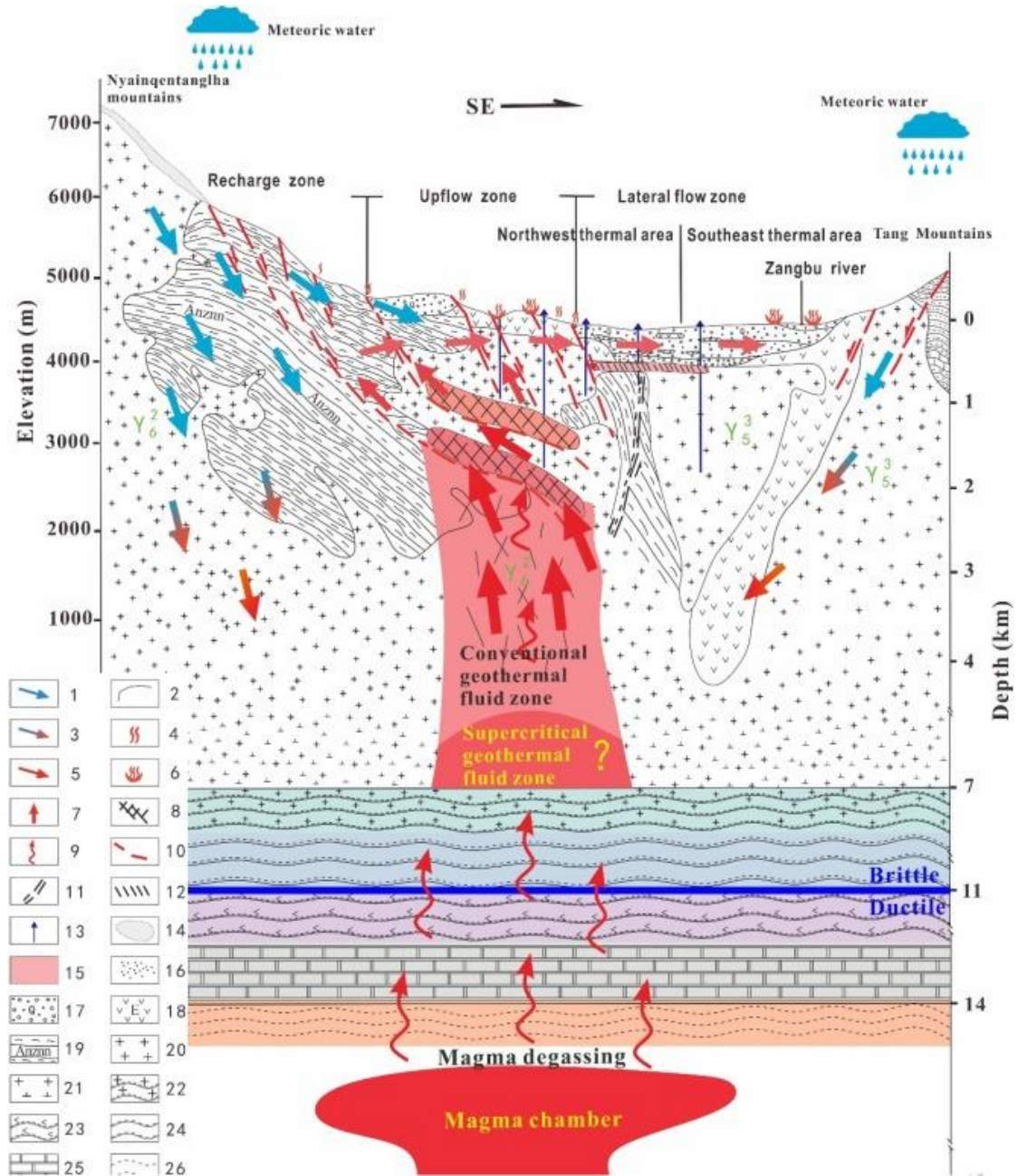
Fig. 3. Circulation model of geothermal water and the speculated petrography of the Yangbajing geothermal field. The numbers in the figure are: 1. infiltration meteoric water; 2. geological boundaries; 3. heating groundwater; 4. steaming ground; 5. lateral flow of geothermal fluid; 6. hot springs; 7. upflow of geothermal fluid; 8. deep fracture granite reservoir; 9. deep volatiles; 10. faults; 11. slip fault system; 12. shallow fracture reservoir; 13. geothermal well; 14. snow; 15. geothermal reservoir; 16. Quaternary pore type reservoir; 17. Quaternary loose bed; 18. Eocene–Oligocene pyroclastic rocks;
19. Precambrian metamorphic core complex; 20. granite; 21. granodiorite; 22. granite gneiss; 23. granoamphibolite; 24. gneiss; 25. marine carbonate rocks; 26. migmatite. This schematic diagram is based on Searle et al., 1987, Dor et al., 1997, Zhao et al., 2001, Craw et al., 2005, Kapp et al., 2005, Lee and Whitehouse, 2007, Wu et al., 2007; Hacker et al., 2014; Wang et al., 2014, Weller et al., 2016; Gébelin et al., 2017; Wu et al., 2021.

3. Sampling and analysis

Several types of fluid samples were collected from the Yangbajing area in 2020 for the chemical and isotopic analyses: four geothermal water, two cold groundwater, four condensate water, three surface water, and four gas samples. Also, parameters such as the pH, temperature (℃), total dissolved solids (TDS) (ppm), oxidation–reduction potential (ORP) (mV), and electrical conductivity (EC) (μS/cm) of the water samples were measured at the field using handheld meters (HQ40D, Hach). The sampling locations are shown in Fig. 2b. The borehole gas samples were collected using the water displacement method (Tian et al., 2019) after the geothermal fluids were separated using wellhead water–steam separators, following the method described by Arnórsson et al. (2006). A 50-mL narrow-mouth glass bottle was filled with geothermal water from the sample well and submerged upside down into the thermal water in a barrel. Then, a tube linked to the separator was inserted into the glass bottle, and the water in the bottle was displaced by the gas. The bottle was plugged with a silicone stopper and sealed with an aluminum cap after the water in the bottle was discharged to two-thirds of the bottle's volume. The sampling bottle was sealed upside down in a 500-mL HDPE bottle full of corresponding geothermal water with no headspace to prevent atmospheric contamination of the gas sample. Additionally, we collected four or five parallel samples from each well for the detection of their gas components, noble gas isotopic compositions, and carbon isotopic compositions.

Hydrogen and oxygen isotopes were measured by a laser water isotope analyzer (L1102-I, Picarro). The isotopic ratios were based on the standard of the Vienna Standard Mean Ocean Water (VSMOW). The analytical precisions of δD and $\delta^{18}O$ were 0.5‰ and 0.1‰, respectively. The compositions of the major gas chemical species, including CH_4, CO_2, H_2, N_2, O_2, Ar, He, and H_2S, were determined using a MAT 271 mass spectrometer with relative standard deviations of less than 5% and expressed in percent by volume. $\delta^{13}C–CO_2$ values (with respect to Vienna Pee Dee Belemnite [VPDB]) were obtained using a gas isotope mass spectrometer (Delta VTM, Thermo Finnigan) coupled with an online sample preprocessor (Tian et al., 2019). The measurement error for the ratio of carbon isotope values was ±0.2‰. $^3He/^4He$ and $^4He/^{20}Ne$ ratios were analyzed using a Noblesse noble gas mass spectrometer produced by Nu Instruments, UK. The noble gas isotopic ratio measurement results had errors of less than 7%. These measurements were completed within 1 month after the field works.

4. Results

4.1. Chemical parameters and isotope characteristics of the water

The water types of all the samples were classified as river water, cold groundwater, thermal groundwater, and condensate water (Table 1). All samples in the study were alkaline (pH > 7), and most of the geothermal water had a pH of ~9. The TDS of the geothermal water ranged from 439 to 1754 ppm with an average of 1323 ppm, whereas that of cold water was less than 700 ppm. Most of the geothermal water had a high EC of over 2000 μS/cm,

whereas the cold water had an EC below 1000 μS/cm. Almost all of the water samples had negative ORP values except No. B-02, indicating that those waters are in a reducing environment.

Table 1. Chemical parameters and isotope of the river water, cold groundwater, thermal groundwater, and condensate water of the Yangbajing geothermal system.

No.	Water type	Temp. [℃]	pH	TDS [ppm]	EC [μS/cm]	ORP [mV]	δD/‰	δ^{18}O/‰
B-01	Hot spring	84.7	8.21	1494	2167	−119	−147.13	−17.11
B-02	Geothermal water	65.8	9.38	439	651	18	−160.99	−20.04
B-03	Cold groundwater	29.5	7.73	269	392.1	−84	−158.56	−20.35
B-04	Cold groundwater	11.2	7.52	123	166.8	−67	−152.62	−19.58
B-05	Geothermal water	81.5	8.56	1609	2326	−99	−149.41	−17.42
B-06	Hot spring	81.9	8.76	1754	2556	−87	−150.32	−17.37
B-07	Condensate water	67.6	9.15	1621	2312	−240	−147.88	−18.23
B-08	Condensate water	46.3	9.33	1707	2478	−158	−147.77	−17.81
B-09	Condensate water	54.4	9.22	1761	2542	−180	−152.02	−18.90
B-10	Condensate water	52.3	8.73	1514	2194	−90	−151.71	−18.99
B-11	River water	18.9	7.7	123	166.8	−46	−140.38	−18.87
B-12	River water	32.7	8.1	699	988.9	−38	−142.41	−16.39
B-13	River water	19.3	7.99	161	233.3	−11	−140.39	−18.33

For the geothermal water, the δD and δ^{18}O values were from −160.99‰ to −147.13‰ (mean −151.96‰) and −20.04‰ to −17.11‰ (mean −17.99‰), respectively. For the condensate water, the δD value was from −152.02‰ to −147.77‰ (mean −149.85‰), and the δ^{18}O value was from −18.99‰ to −17.81‰ (mean −18.48‰). Compared with the geothermal waters, the condensate waters were slightly depleted in δ^{18}O because of the fractionation of isotopes during the condensation of two-phase geothermal fluids.

4.2. Chemical and isotopic composition of dissolved gases

The compositions of the dissolved gases are listed in Table 2. The dominant component of the dissolved gases in geothermal water was CO_2 at 68.8%–92.5%, with an average value of 81.4%. N_2 and O_2 were the next most dominant, with the mean values of N_2 and O_2 percentage at 14.7% and less than 10%, respectively. The contents of other gases were low, most of which were less than 1%, with hardly any CH_4. The percentage of H_2S does not exceed 0.5% in the gas. The He content was also less than 0.1%. The N_2/Ar value ranged from 82 to 128.1.

Table 2. Chemical composition (vol%) of gases from the Yangbajing geothermal system.

Sample ID	Depth [m]	H_2	CH_4	N_2	O_2	H_2S	Ar	CO_2	He [ppmV]
B-07	90.1	0.04	0.03	24.19	6.22	0.5	0.26	68.76	5.8

Sample ID	Depth [m]	H_2	CH_4	N_2	O_2	H_2S	Ar	CO_2	He [ppmV]
B-08	300	0.04	0.03	17.95	5.13	0.46	0.22	76.17	58
B-09	206.5	0.01	0.08	10.04	1.43	0.07	0.08	88.29	740
B-10	82	0.01	0.07	6.69	0.63	0.05	0.05	92.5	455

The δ^{13}C–CO_2 values varied slightly, ranging from $-12.3‰$ to $-7.7‰$. The R/R_a values, corrected for the He/Ne ratio of the air (1.13–21.9) (Ozima and Podosek, 2002), ranged from 0.08 to 0.26 Ra except for B-07, which was contaminated by air helium and are not included in the further discussion. The $CO_2/^3$He values varied from 7.24×10^8 to 1.27×10^{11} while the $CH_4/^3$He values range between 6.35×10^5 and 4.1×10^7 (Table 3).

Table 3. He and C isotopic characteristics and compositions of the geothermal gases from the Yangbajing geothermal system.

Sample ID	R/R_a	R_c/R_a[a]	$^3He/^4He$	$^4He/^{20}Ne$	He inventory[b] (%)			$\delta^{13}C$-CO_2	$CO_2/^3He$	$CH_4/^3He$	CO_2 inventory[c] (%)			References
					Air	Mantle	Crust				Mantle	Limestone	Sediments	
Empty Cell	Empty Cell	Empty Cell	Empty Cell	Empty Cell	Air	Mantle	Crust	Empty Cell	Empty Cell	Empty Cell	Mantle	Limestone	Sediments	Empty Cell
B-07	1	1	1.41×10^{-6}	0.33	0.96	0.01	0.03	−11.66	8.41×10^{10}	4.10×10^7	0.02	0.57	0.41	This study
B-08	0.21	0.14	2.4×10^{-7}	3.5	0.09	0.01	0.9	−12.29	5.47×10^{10}	2.48×10^7	0.03	0.54	0.43	
B-09	0.08	0.08	1.18×10^{-7}	3280	0	0.01	0.99	−7.83	1.01×10^{10}	8.88×10^6	0.15	0.59	0.26	
B-10	0.09	0.09	1.19×10^{-7}	353	0	0.01	0.99	−8.35	1.71×10^{10}	1.25×10^7	0.09	0.62	0.29	
ZK304	–	0.16	2.23×10^{-7}	514.6	0	0.02	0.98	−8.76	5.63×10^{10}	–	0.03	0.65	0.32	
ZK313	–	0.09	1.22×10^{-7}	286.1	0	0.01	0.99	−9.88	1.27×10^{11}	–	0.01	0.63	0.36	
ZK324	–	0.14	1.89×10^{-7}	971	0	0.02	0.98	–	–	–	–	–	–	
ZK329	–	0.12	1.72×10^{-7}	627.6	0	0.02	0.98	−7.72	4.49×10^{10}	3.97×10^7	0.03	0.68	0.29	
ZK353	–	0.11	1.58×10^{-7}	812.3	0	0.01	0.99	–	–	–	–	–	–	Zhao et al., 1998
ZK354	–	0.17	2.31×10^{-7}	479.9	0	0.02	0.98	−11.3	1.22×10^{10}	–	0.12	0.50	0.38	
ZK355	–	0.13	1.81×10^{-7}	477.5	0	0.02	0.98	−10.3	6.88×10^{10}	–	0.02	0.61	0.37	
ZK357	–	0.18	2.49×10^{-7}	114	0	0.02	0.98	–	–	–	–	–	–	
ZK4001	–	0.26	3.63×10^{-7}	7002.2	0	0.03	0.97	−11	7.24×10^8	6.35×10^5	–	–	–	

a

R_c/R_a is the air-corrected He isotope ratio $= [(R/R_a)X - 1]/(X - 1)$, where X is the air-normalized respective ratio: $X = (^4He/^{20}Ne)_{measured}/(^4He/^{20}Ne)_{air}$. Air:

$(R/R_a = 1, ^4He/^{20}Ne = 0.318)$ (Sano and Wakita, 1985).

b

Endmembers: Air: $(^3He/^4He) = 1.4 \times 10^{-6}$, $(^4He/^{20}Ne) = 0.318$; mantle: $(^3He/^4He) = 1.1 \times 10^{-5}$, $(^4He/^{20}Ne) = 1000$; crust: $(^3He/^4He) = 1.5 \times 10^{-8}$,

$(^4He/^{20}Ne) = 1000$ (Sano and Wakita, 1985).

c

Mantle: $\delta^{13}C = -6.5‰$, $CO_2/^3He = 1.5 \times 10^9$; limestone: $\delta^{13}C = +1.5‰$, $CO_2/^3He = 1 \times 10^{13}$; sediments: $\delta^{13}C = -30‰$, $CO_2/^3He = 1 \times 10^{13}$ (Sano and Marty,

1995).

4.3. Applications of gas geothermometers

4.3.1. Dissolved gas geothermometer

Based on gas–gas and gas–rock reactions, the relationships between gas components could be used to evaluate the physical and chemical states of geothermal reservoirs. However, it is recognized that gas geothermometers have some characteristics that are difficult to control. A significant hurdle to using gas component geothermometers is the redox state of fluids, especially for reactive phases such as H_2S, H_2, CH_4, or CO, which are sensitive to redox potential. Highly immature geothermal areas are closely related to active volcanoes (Giggenbach, 1987). They usually have acidic, sulfate chloride waters; and an assembly of highly oxidizing alteration minerals, such as gypsum and alunite. In contrast, mature geothermal areas have neutral-pH discharges; low sulfuric acid, chlorine-dominated hot waters; potassium feldspar and potassium mica (muscovite) symbiosis; and calcite alteration to produce Ca–Al–silicate rock. For more oxidized states, such as those with gypsum and alunite, CO_2/CH_4 geothermometers are less suitable. Moreover, Giggenbach (1993) showed that R_H is a parameter that quantifies the redox state, with $R_H = -2.8$ indicating a steady-state chemical equilibrium of fluid components.

The gas system H_2O–CO_2–H_2–CO–CH_4 is an effective geothermometer widely used for geothermal fluids (Chiodini and Marini, 1998). However, the H_2O steam in a sample pool is affected by boiling as geothermal water flows to the surface. Also, CO undergoes oxidation after mixing with shallow aquifer during the ascent of geothermal fluids. Therefore, we used the CO_2–CH_4–H_2 system in the geothermal system of Yangbajing. A redox-condition independent diagram (Fig. 4; H_2/Ar^* vs. CH_4/CO_2) was combined to determine the gas equilibrium temperature, and the degree of full redox equilibrium was attained. In typical situations, the temperature-controlled FeO–$FeO_{1.5}$ redox pair is the most suitable buffer in a hydrothermal system with $R_H = -2.8$. The CH_4–

CO_2 relationship conforms to the Fischer–Tropsch equation:

$$(1) \quad CH_4 + 2H_2O \leftrightarrow CO_2 + 4H_2$$

thus, the $\log(X_{CO2}/X_{CH4})$ value (where X_{CO2} and X_{CH4} are the CO_2 and CH_4 fractions, respectively) resulting from liquid phase boiling can be expressed by the following formula:

$$(2) \quad \log\frac{X_{CH4}}{X_{CO2}}^v = 4R_H + \frac{5181}{T_K}$$

here, $R_H = \log(H_2/H_2O)$. Thus, in the liquid phase, $\log(X_{CO2}/X_{CH4})$ also depends on the coefficients of the CH_4 and CO_2 partition (B_{CO2} and B_{CH4}) between gases and liquids, as follows:

$$(3) \quad \log\frac{X_{CH4}}{X_{CO2}}^L = 4R_H + \frac{5181}{T} + \log B_{CO2} - \log B_{CH4}$$
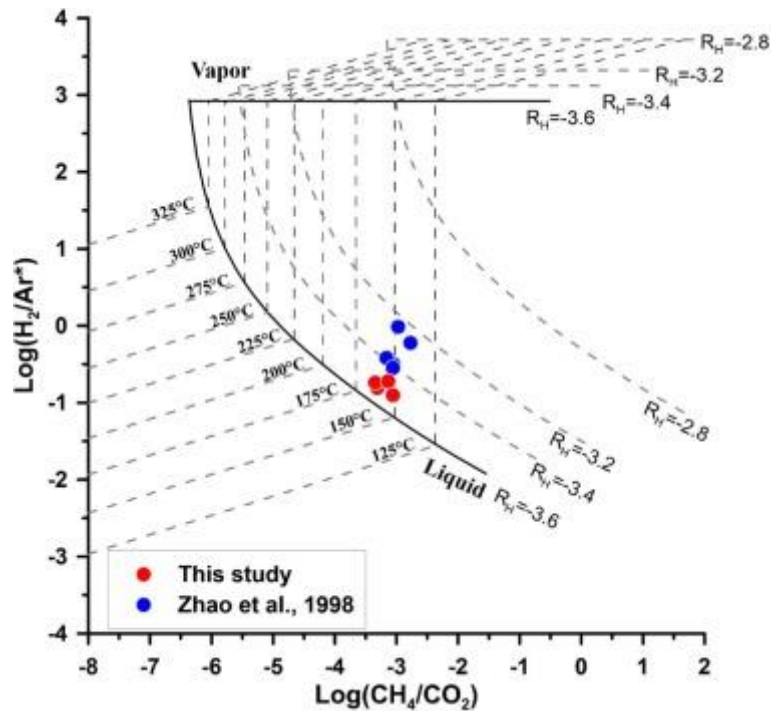
Fig. 4. Log(H_2/Ar*) vs. log(CH_4/CO_2) for the Yangbajing gases. The lines shown in the diagram represent isotherms and some redox buffers usually effective in volcanic–hydrothermal environments. Modified after Giggenbach (1987).

With the assumption that Ar in a geothermal fluid is consistent with air-saturated water (ASW) (Giggenbach, 1987), a geological thermometer based on the H_2–Ar–CH_4–CO_2 gas–liquid dissolution equilibrium relationship was established. When water boils, the relationship between hydrogen and Ar is as follows:(4)$\log \frac{X_{H2}}{X_{Ar}}v = R_H + 6.52$ in the liquid phase, the characteristic formula is:(5)$\log \frac{X_{H2}}{X_{Ar}}L = R_H - \log B_{H2} + 6.52$ where B_{H2} is the equilibrium coefficient of H_2 between the gas and liquid phases. Therefore, the log(X_{H2}/X_{Ar}*) vs. log(X_{CH4}/X_{CO2}) diagram (Giggenbach, 1993) shows that the R_H value in the gas–liquid equilibrium is −3.6 to −2.8, which also represents a temperature increase from 125 ° C to 374 ° C (Fig. 4 in Giggenbach (1993)). The four formulas above show B_{CO2}, B_{CH4}, and B_{H2} values as reported by Sepúlveda et al. (2007). The thermometer diagram of the CO_2–CH_4–H_2 system (Fig. 4) shows that the solution equilibrium temperature of the Yangbajing geothermal field tends to about 140 ℃–160 ℃, and the R_H value is between −3.2 and −3.6.

4.3.2. Soil CO_2 flux geothermometer

Hot springs, especially those formed by steam-heated meteoric water, are usually of the acid sulfate variety. These hot water samples contain limited reservoir chemistry information and are not perfect for geochemical geothermometers (Arnórsson, 2000, Mukherjee and Singh, 2020). Thus, obtaining sufficient samples and reconstructing the composition of the parent geothermal fluid by correcting the mixing and degassing processes are

necessary for these hydrochemical samples to be usable as geothermometers (Fournier, 1977, Palandri and Reed, 2001). A common problem with geochemical thermometers is that geothermal water easily rebalances with surrounding rocks as it rises from the reservoir to the surface. They also easily precipitate and dissolve, making deviations common. Thus, the dissolved gas equilibrium geothermometer may have some deviations due to easy air mixing during sampling or the enrichment of non-condensable gas due to vapor condensation (Arnórsson and Gunnlaugsson, 1985).

Harvey et al. (2017) developed a new gas geothermometer using soil CO_2 flux data from five geothermal systems (Wairakei, Tauhara, Rotokawa, Ohaaki, and Reporoa) in the Taupo Volcanic Zone. This geothermometer makes up for the problem of conventional gas geothermometers being easily polluted by air. In this method, the spatial distribution value of the soil CO_2 flux in the geothermal anomaly area was first obtained using the accumulation chamber method. Then, the soil heat flux was obtained according to the method of Hochstein and Bromley (2005):(6)$Q_{tot} = \alpha Z_{bp}/Z_o - \beta$where Q_{tot} is the total heat flux (W m^{-2}), α (185 W m^{-2}), and β (0.757) are empirically

derived constants, Z_{bp} is the boiling depth (for pure water at local elevation), and Z_o is the unit of depth (1 m). Then, the steam flux in the geothermal area can be as follows:(7)$F_{stm} = Q_{tot}h_s - h_w - 1$where F_{stm} is the steam flux (kg m^{-2} s^{-1}), Q_{tot} is the inferred heat flux (Eq. (6)), h_s is the enthalpy of steam at the local boiling point (kJ kg^{-1}),

and h_w is the enthalpy of liquid water at ambient conditions (kJ kg^{-1}). The CO_2 concentration in the steam is then

converted into temperature:(8)$T_{CO2Flux} = -44.1 + 269.25R - 76.88R^2 + 9.52R^3$where $T_{CO2Flux}$ is the reservoir temperature (℃), and R is the logarithm of the CO_2 concentration in the steam supplying the thermal area (log mmol kg^{-1}) from the CO_2 flux measurements and Eq. (7). Eq. (8) applies to high-temperature geothermal reservoirs

hosted in mafic to silicic rocks (Arnórsson and Gunnlaugsson, 1985). This method should also be effective in the Yangbajing area.

Soil CO_2 flux and soil temperature data from Zhang, 2015 have been used in the Yangbajing geothermal field to estimate its reservoir temperature (Table S2). The data shows two different geothermal zones in the Yangbajing geothermal field (Fig. 3). Following the process of Harvey et al., (2017), we calculated the reservoir temperature in the north and south geothermal areas; the reservoir temperature in the whole geothermal field was also calculated, as shown in Fig. 5. In addition, according to the frameworks from Harvey et al. (2017), we adopted the results of Seward et al. (2018) for the soil heat flux formula and calculated the reservoir temperatures in the different geothermal areas of Yangbajing again. The results are also shown in Fig. 5. According to the method of Hochstein and Bromley (2005), the temperature in the southeast of Yangbajing is between 55 ℃ and 267 ℃, with an average of 208 ±42 ℃; the temperature in the northwest is between 175 ℃ and 342 ℃, with an average of 275 ±33 ℃. The average reservoir temperature of the entire geothermal area of Yangbajing is 248 ±48 ℃. When the soil heat flux formula of Seward et al. (2018) is adopted, the temperature in the southeast is between 80 ℃ and 276 ℃, with an average value of 220 ±39 ℃. The temperature in the geothermal area of northwest Yangbajing is between

186 ℃ and 348 ℃, with an average of 282 ±31 ℃. The average reservoir temperature in the whole geothermal area is 257 ±45 ℃.
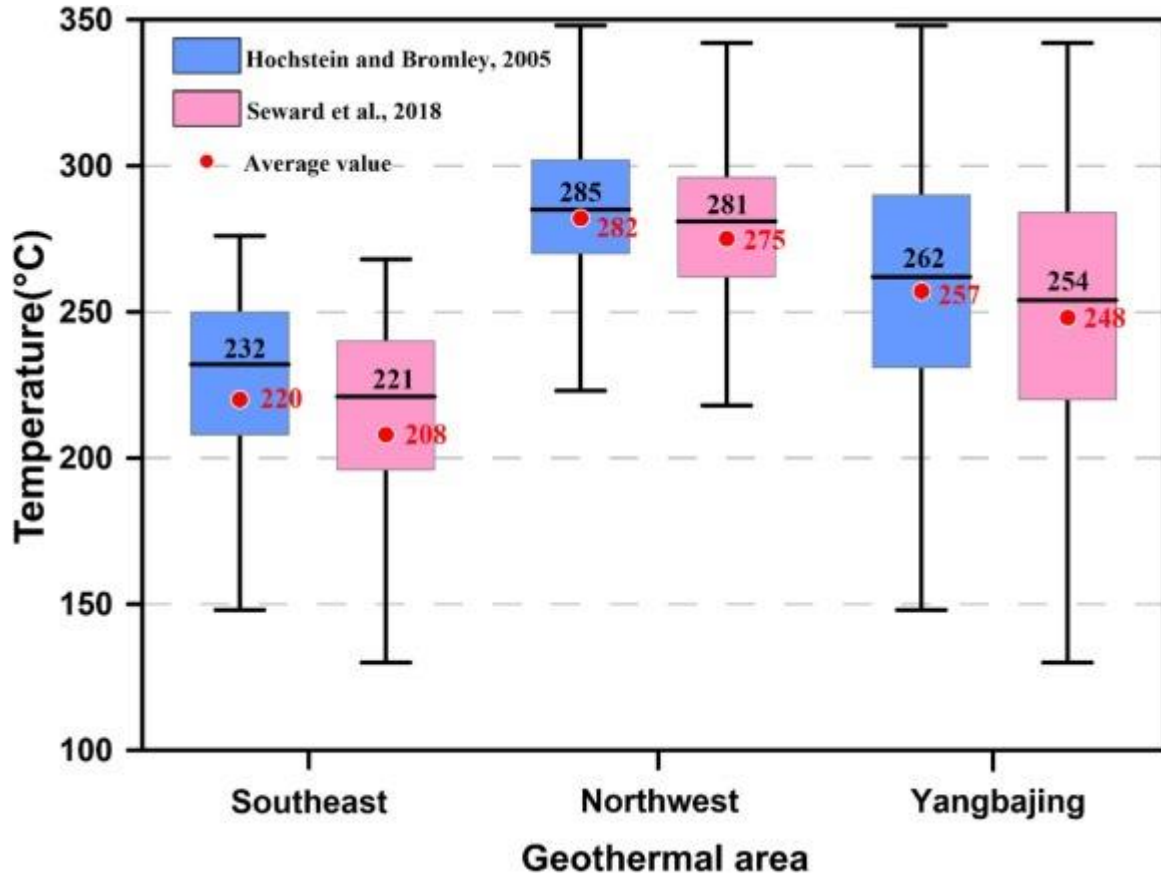

Fig. 5. The reservoir temperature estimated from the soil CO_2 flux in the Yangbajing geothermal field.

4.3.3. Noble gas geothermometer

Among geothermal fluid geothermometers, many empirical gas geothermometers have been developed earlier, such as those for CO_2 and H_2S (Arnórsson and Gunnlaugsson, 1985) or the CO_2–H_2S gas equilibrium system (Arnórsson and Gunnlaugsson, 1985, Chiodini and Marini, 1998). There are also CO_2/Ar and H_2/Ar gas ratios, among others (Arnórsson, 2000), these gas geothermometers are useful to some degree. However, they are all based on the theoretical assumption that the gas compositions or gas ratios in a geothermal reservoir are controlled by gas–gas equilibrium or gas–mineral thermodynamic equilibrium and that this equilibrium is fixed when the local thermal fluid rises from the reservoir to the surface (Giggenbach, 1980). Some problems arise with this assumption, such as the chemical rebalancing of some of the reacting gases as they rise and the condensation and boiling of shallow vapors, which change the compositions of the gases. These conditions limit the use of empirical geothermal gas geothermometers. Further, one more critical problem is the difficulty of distinguishing between the reservoir state and secondary processes (Stefánsson, 2017). Recently, Byrne et al. (2021) developed a noble gas geothermometer by adopting Icelandic geothermal gas data based on the thermodynamic equilibrium process of noble gas dissolution in geothermal reservoirs. The most typical characteristic of noble gases is that they almost do not react

with surrounding rocks. Thus, their rise from the reservoir to the surface is basically only controlled by the thermodynamic equilibrium of dissolution. Therefore, they have a broader application prospect than those of empirical geothermometers.

This method assumes that the <u>isotope fractionation</u> of noble gases (Ne, Ar, Kr, and Xe) between gases and liquids is controlled by temperature. Furthermore, the distribution relationship between noble gas concentration and saturated groundwater can be deduced as follows:(9)$[i]v=[i]aswKDi(T)KDi(T)-1Xv+1$where the partitioning can be described at equilibrium by the vapor–liquid distribution coefficient. This coefficient is defined as the ratio between the mole fractions of a species (i) in the vapor (v) and liquid (aq) phases, which is the abundance in the initial ASW phase and the subsequent vapor and liquid phases, respectively. In an extreme case, when $X_v = 0$, the relation can be presented as:(10)$iv=iaswKDi(T)$

On the basis of this relationship, the functional relationship between the gas isotopes of Ne, Ar, Kr, and Xe and temperature can be established. Then, the inverse function relationship between the gas isotope concentrations can be established:(11)$Ti=KDi-1[i]v[i]asw$the temperature of the geothermal reservoir can then be obtained. However, the single gas isotope estimation method does not consider the influence of <u>atmospheric composition</u> on isotope mixing. Therefore, <u>Byrne et al. (2021)</u> also corrected the concentration of gas isotopes in the context of atmospheric mixing:(12)$KDjKDi-1[i]vcorr[i]asw+[i]vcorrM-[j]air[i]air-M=0$the atmospheric correction for noble gas isotope concentration is represented by [i]vcorr, and the gradient of the mixing line is as follows:(13)$M=j/isample-j/iair1/[i]sample-1/[i]air$by integrating the mixing line, the mixing proportion and the corresponding mixing reservoir temperature can be obtained.

We adopted the noble gas data of <u>Zhao et al. (2001)</u> for the Yangbajing geothermal field and estimated the temperatures of single noble gases, as shown in <u>Fig. 6</u>. The relation diagram of ^{20}Ne, ^{84}Kr, and ^{36}Ar shows that the gas temperature of the geothermal field is concentrated on the evolutionary equilibrium line at 220 ℃–260 ℃. Considering that these geothermal gas samples could easily mix with atmospheric components, we also used a mixed noble gas geothermometer to estimate the reservoir temperature of the Yangbajing geothermal field, as shown in <u>Fig. 7</u>. As can be seen from the figure, the reservoir temperature is basically concentrated at 240 ℃–260 ℃, and the proportion of atmospheric mixing is 0.2 on average. This ratio is closely related to that of the samples from the high-altitude area of Yangbajing.
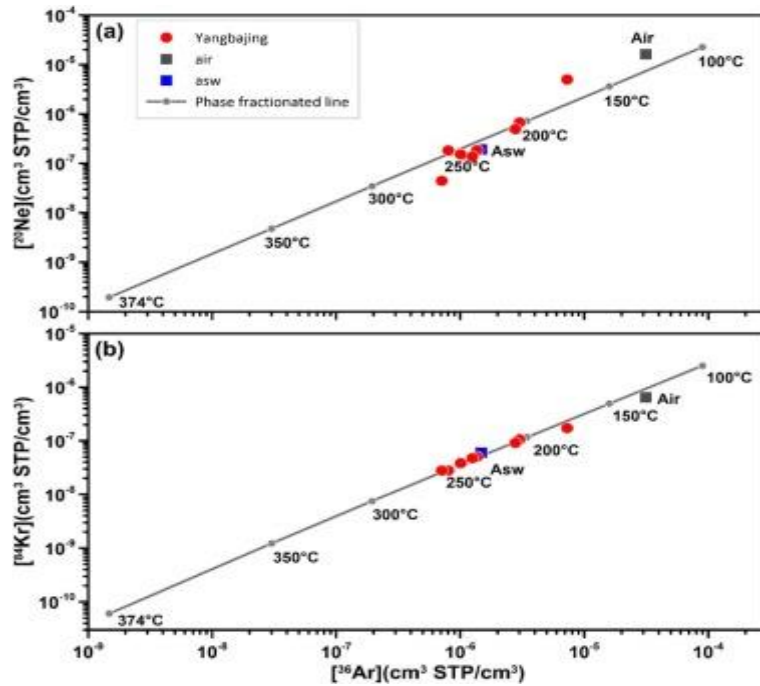
Fig. 6. Abundances of atmosphere-derived noble gas isotopes. The gray lines represent the predicted composition of a vapor phase fractionated from an initial ASW phase over a range of temperatures. Panels (a) and (b) show the good fit of ^{20}Ne, ^{84}Kr, and ^{36}Ar abundances to the estimated fractionation line with temperatures ranging from 220 ℃ to 260 ℃.
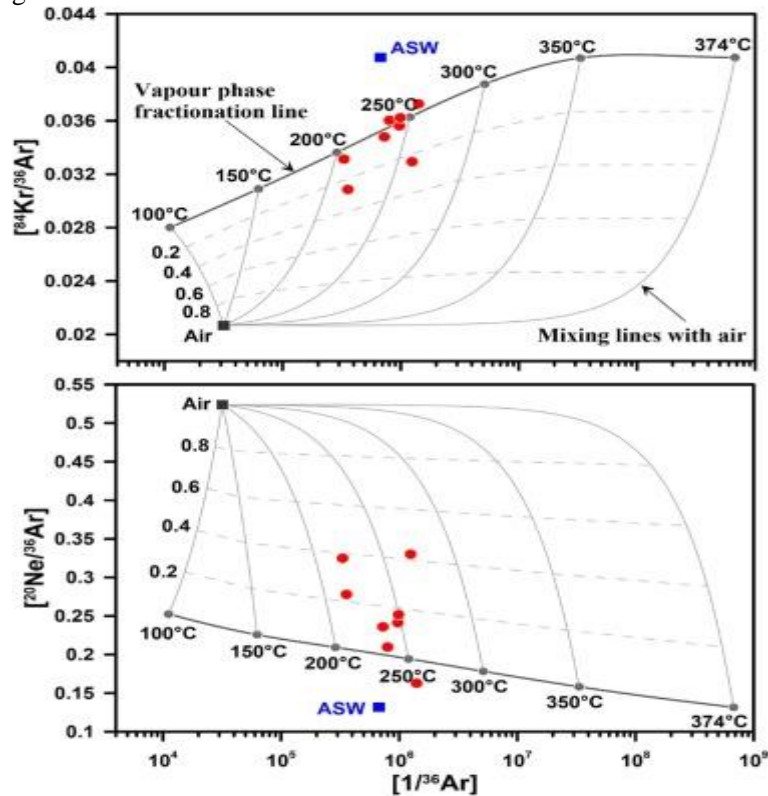

Fig. 7. Plot of ^{84}Kr/^{36}Ar and ^{20}Ne/^{36}Ar vs. 1/^{36}Ar in panels (a) and (b), respectively. The plot shows the mixing relationships between the expected initial vapor phase composition upon fractionation at various temperatures and the air value.

5. Discussion

5.1. Sources of geothermal water

The δD vs. δ^{18}O relationship in the Yangbajing geothermal area was plotted based on the data from the collected samples and the compiled data (Table S1) (Fig. 8). The cold groundwater, thermal groundwater, and condensate water were near the global meteoric water line (GMWL) (Craig, 1961) and the local meteoric water line (LMWL) (Tan et al., 2014), indicating their meteoric water source. The magmatic water (δ^{18}O = 10 ±2‰, δD = −20 ± 10‰) from Giggenbach (1992) and the snowmelt water from Guo et al. (2010) are plotted as two endmembers in Fig. 8. Most of the geothermal water in the Yangbajing geothermal field was distributed in the mixing zone of the magmatic water and meteoric water. The average mixing ratio with magmatic water was about 25%. Fig. 8b also shows that some of the geothermal water might have been mixed with cold groundwater.
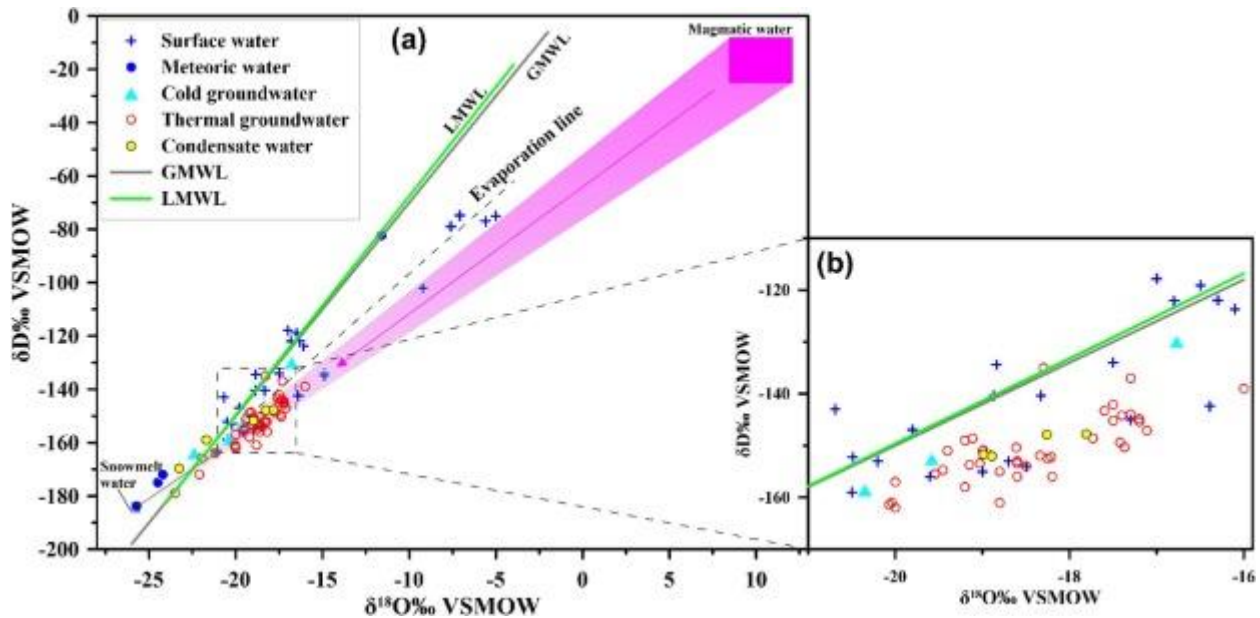

Fig. 8. δD and δ^{18}O (‰VSMOW) values for the water samples collected from the Yangbajing area. GMWL: global meteoric water line (Craig, 1961); LMWL: local meteoric water line (Tan et al., 2014).

Isotope exchanges between water and rock often result in "oxygen shift" in many high-temperature geothermal systems (Giggenbach, 1992). However, the oxygen isotope shift in the Yangbajing geothermal field was not observable, which might be because of mixing with magmatic water, weak water–rock interactions, or both (Pichler, 2005). The "horizontal only" shift of δ^{18}O to the right due to water–rock interactions might be reversed by isotope exchange between CO_2 and H_2O during CO_2 degassing. Oxygen isotope shifts to the left have been observed in some CO_2-rich geothermal systems, while most geothermal systems in the Himalaya geothermal belt are rich in CO_2 (Girault et al., 2014, Wang et al., 2021). Fig. 8a shows that both δD and δ^{18}O shifted right slightly, indicating that they were dominated by mixing with magmatic water. On the basis of the δD and δ^{18}O relationship,

we suggest that a small amount of the geothermal fluid beneath the Yangbajing geothermal area was affected by magmatic water at depth.

5.2. The origin of N_2 and Ar

The probable nitrogen sources in the geothermal area are (a) the atmosphere, (b) the mantle, including the mantle wedge and the subducting oceanic crust, and (c) sediments (both subducted oceanic deposits and continental crust) (Inguaggiato et al., 2004). Nitrogen sources in the crust usually involve biological activities (NH_4), deposition, and diagenesis (Bebout et al., 2013, Mysen, 2019, Mukherjee and Singh, 2021). As can be seen from the N_2–He–Ar triangle diagram of the gas components (Fig. 9), the N_2/Ar ratios (ranging from 82 to 128.1) of the newly collected samples were slightly higher than that of ASW (40) and generally similar to that of the air (83). These indicate that these ratios comprise atmospheric sources and excess nitrogen (Table 2). Almost all the samples were close to the He corner within a narrow area (shadow in Fig. 9), indicating mixing with deep-seated nitrogen sources (excess nitrogen), probably crustal metamorphic rocks or mantle volatiles (Evans et al., 2008, Zhang et al., 2017b). Considering the abundant ^{4}He from crustal radioactive activities, we inferred that most of the deep-seated N_2 of the hot spring gases likely has a crustal genesis from metasedimentary sources.
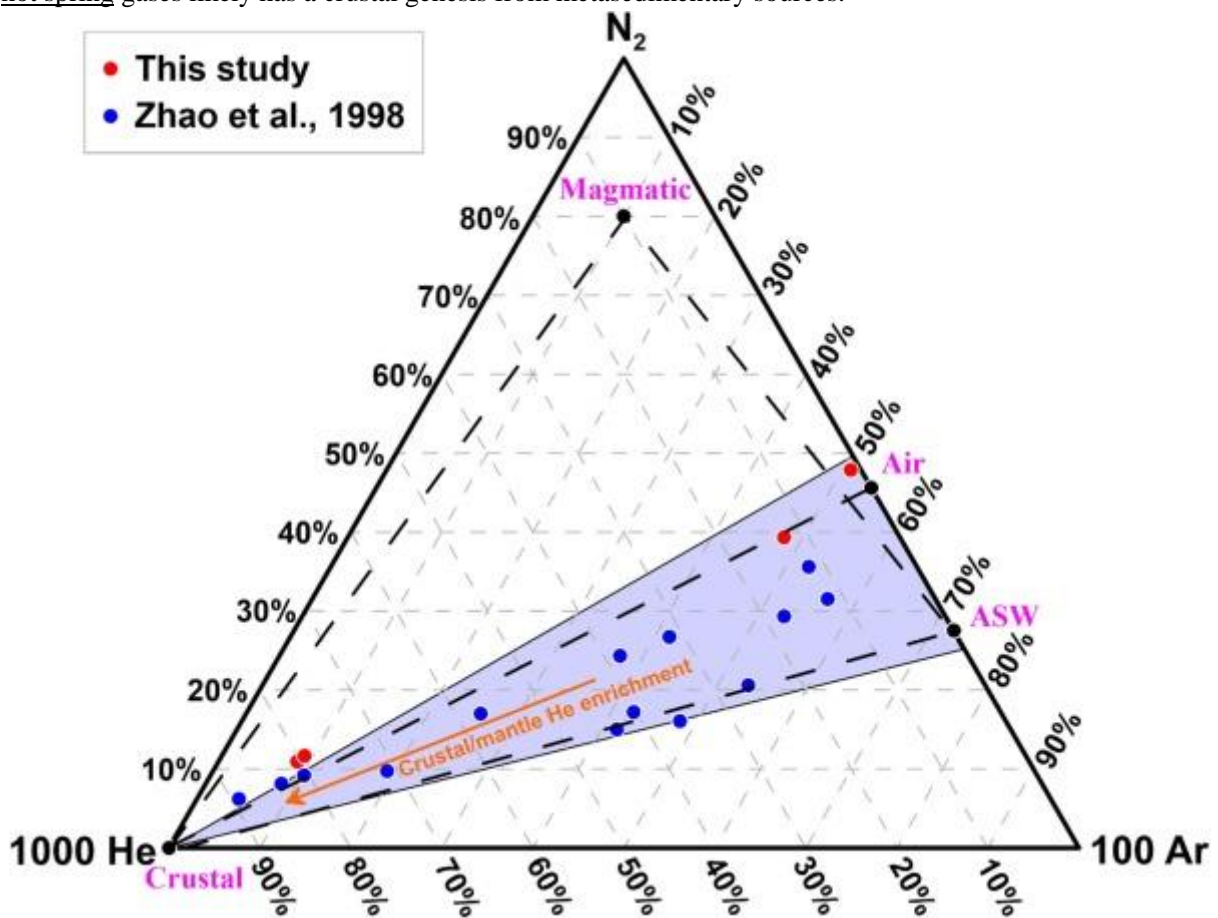

Fig. 9. The N_2–He–Ar ternary diagram of the Yangbajing geothermal field (modified from Giggenbach, 1993).

5.3. Sources of He and CO_2

5.3.1. The origin of He

He is a noble gas element involving only physical processes (i.e., no chemical reactions) during the ascent of gases. Therefore, the He isotope is an important indicator in determining the characteristics of source regions. According to current knowledge, the endmembers of He sources are relatively clear: crustal-source ^4He, which is mainly produced by alpha decay of $^{235,238}U$ and ^{232}Th in the crust, and mantle-source ^3He, which is dominated by degassing. The $^3He/^4He$ (R) value is generally 0.02 to 0.1 Ra in cases with almost no mantle helium mixed in the continental crust. These low $^3He/^4He$ values thus reflect the strong radiogenic ^4He generation in the crust (Ballentine and Burnard, 2002). The R value of mid-ocean ridge basalts (MORBs) is generally 8 ±1 Ra, indicating the existence of primordial ^3He at the beginning of the Earth's formation (Graham, 2002). Thus, the samples' R values between 0.1 and 8 Ra generally indicate a mixture of the mantle- and crust-derived helium. As fluids gradually rise from deep to shallow depths, the helium signal of the mantle becomes weaker (Ballentine and Burnard, 2002).

Previous studies on helium in the Tibetan Plateau (Yokoyama et al., 1999, Hoke et al., 2000) showed that only a very small proportion of mantle-derived helium (<5%) was found between the Bangong–Nujiang suture zone and the Yarlung Zangbo suture zone (IYSZ). To the south side of IYSZ, helium is purely crust-derived. Mantle helium is mainly injected into the crust by the upwelling of the asthenosphere. In the IYSZ, the influence of mantle fluid gradually decreases southward until it is replaced by crust-derived helium at about 100 km north (Hoke et al., 2000, Newell et al., 2008). For the Yangbajing area, the $^3He/^4He$ value was very low (generally less than 0.2 Ra) (Fig. 10). This is much lower than the R values of hot spots or plumes (15–30 Ra; Lupton, 1983), the depleted mantle (8 ±1 Ra), and oceanic island arcs (7.4 ±1.5 Ra; Sano and Fischer, 2013). This indicates a dominant crustal source with little mantle-derived helium.
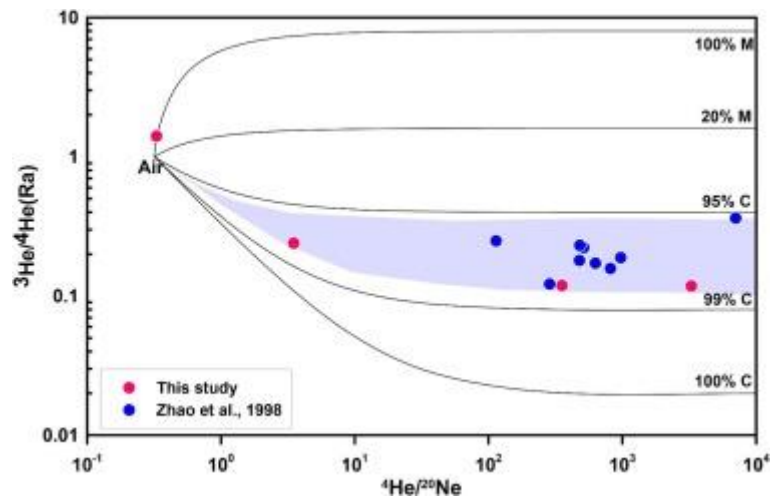

Fig. 10. The $^3He/^4He$ vs. $^4He/^{20}Ne$ gas relationship from the Yangbajing geothermal field (modified from Sano and Marty, 1995). Abbreviation: C, Crust; M, Mantle.

The relationship between ^{3}He/^{4}He and ^{4}He/^{20}Ne (Sano and Wakita, 1985) is adopted in this paper to quantitatively determine the helium source, and the formulas are as follows:$\frac{H3eH4e}{sample}=\frac{H3e}{H4e}A\times fA+\frac{H3e}{H4e}M\times fM+\frac{H3e}{H4e}C\times fC1$ $\frac{H4e}{N20e}sample=fA\frac{H4e}{N20e}A+fM\frac{H4e}{N20e}M+fC\frac{H4e}{N20e}C$ $fA+fM+fC=1$ where A (air), M (mantle), and C (crust) are the endmembers with the following values: air: (^{3}He/^{4}He) = 1.4 $\times 10^{-6}$, (^{4}He/^{20}Ne) = 0.318; mantle: (^{3}He/^{4}He) = 1.1 $\times 10^{-5}$,

(^{4}He/^{20}Ne) = 1000; crust: (^{3}He/^{4}He) = 1.5 $\times 10^{-8}$, (^{4}He/^{20}Ne) = 1000 (Sano and Wakita, 1985). (^{3}He/^{4}He)$_{sample}$ and

(^{3}He/^{4}Ne)$_{sample}$ are the measurement values. fA, fM, and fC are the helium ratios in air, mantle, and crust, respectively. The results listed in Table 3 show that more than 97% of He is crust-derived. According to the tectonic background, as Yangbajing is located at the boundary between the crust- and mantle-derived helium (Hoke et al., 2000), it is more or less affected by the upwelling of asthenosphere mantle-derived helium ($\sim$3%) into the crust. The crust-derived helium originated from the decay of radioactive elements (Yokoyama et al., 1999, Hoke et al., 2000) such as U ($\sim$3 ppm), Th ($\sim$20 ppm) in the country-rock while there are lots of granite at the Yangbajing area (Li et al., 2020).

5.3.2. The origin of CO_2

The relationship between δ^{13}C–CO_2 and CO_2–He in gases is an effective tracer to identify the source of CO_2. The δ^{13}C value in the Yangbajing area ranged from -12.29‰ to -7.72‰, which was between those of marine

carbonates (0 ± 2‰) and crustal sediments (-30 ± 10‰) (Tardani et al., 2016), suggesting a possible mixture of

the two. In addition, Fig. 11 shows that CO_2 in the Yangbajing area may also contain a small amount of MORB components. The samples with high δ^{13}C values and CO_2/^{3}He ratios were largely associated with carbonate rocks (CO_2/^{3}He = 10^{13}, Sano and Marty, 1995).
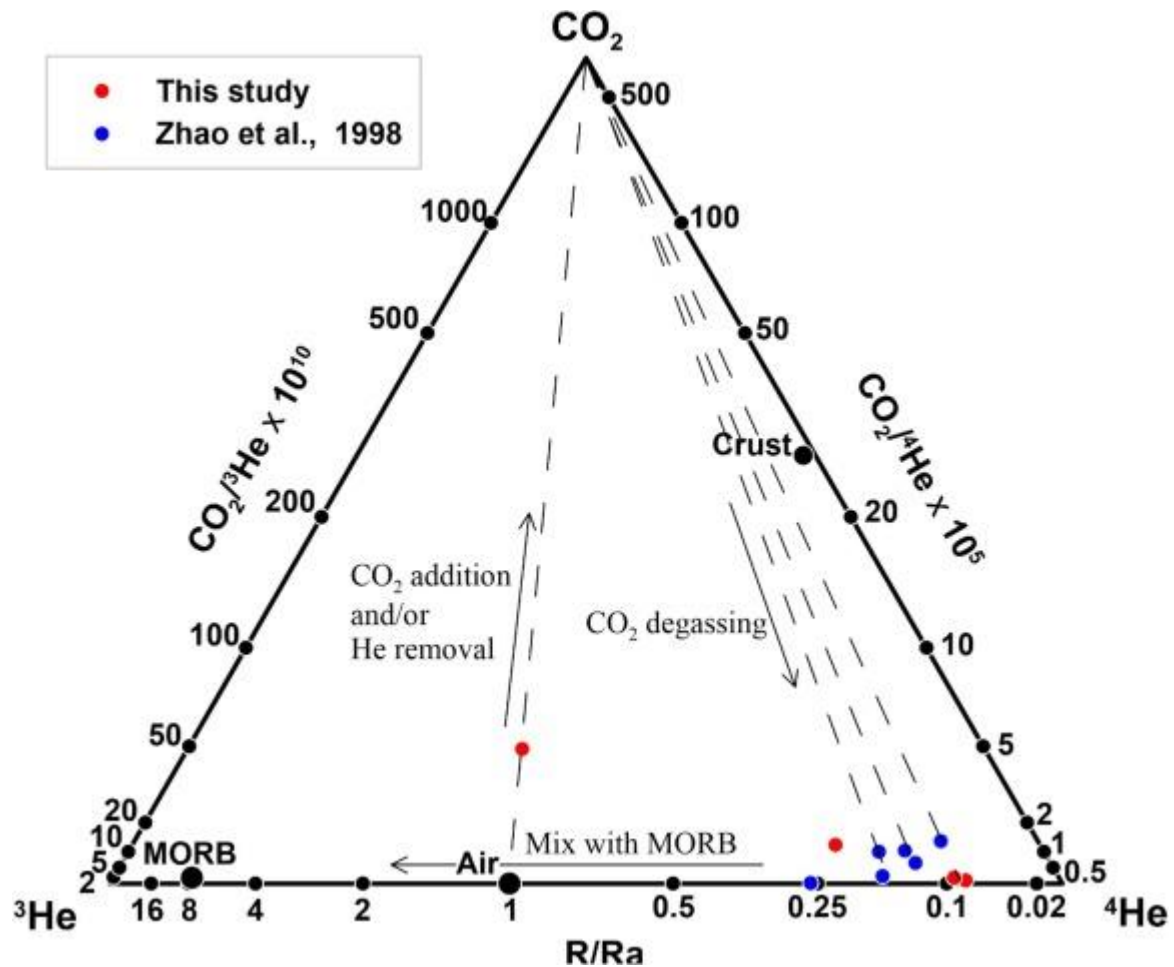
Fig. 11. The CO_2–^3He–^4He ternary diagram of the gases from the Yangbajing geothermal field (modified from Giggenbach, 1993).

Sano and Marty (1995) established a three-terminal mixed model of C–He isotopes, which can identify different endmembers and estimate the proportion of each endmember, especially for those hydrothermal fluids with high CO_2 content. The three endmembers in this study were as follows: mantle, carbonate rock, and sediments. We assumed that the mantle portion is a MORB-type mantle to simplify the calculation. The values of each endmember were $\delta^{13}C = -6.5 \pm 2.5‰$ and $CO_2/^3He = 2 \times 10^9$ for the mantle portion, $\delta^{13}C = 0 \pm 2‰$ and $CO_2/^3He = 10^{13}$ for carbonate, and $\delta^{13}C = -30 \pm 10‰$ and $CO_2/^3He = 10^{13}$ for sediments. The formulas are as follows:C13C12sample=C13C12M×fM+C13C12C×fC+C13C12S×fS1C12/H3esample=fMC12/H3eM+fCC12/H3eC+fSC12/H3eSfM+fC+fS=1the subscripts sample, M, C, and S, refer to the measurement values of the sample, mantle, carbonate rocks, and sediments, respectively. Fig. 12 shows that the samples in the Yangbajing area (except ZK4001) basically fall within the limits of the mantle, carbonates, and sediments. This indicates that these samples only experienced weak He–CO_2 fractionation, which also indicates the effectiveness of calculating the mixing ratios of the three endmembers. The abnormal sample ZK4001 will be discussed later.
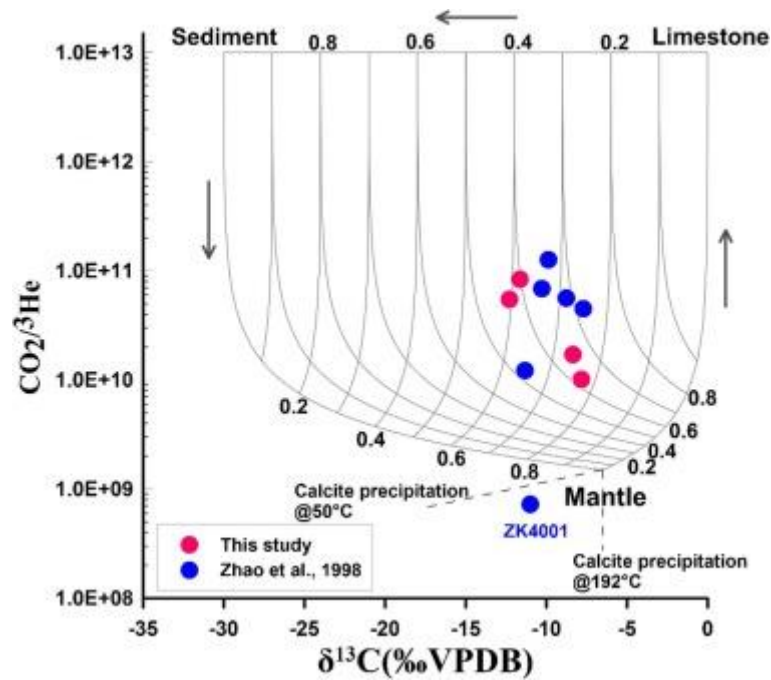
Fig. 12. The δ¹³C–CO₂/³He relationship of the gases from the Yangbajing geothermal field (modified from Sano and Marty, 1995). Doted lines represent predicted trends of calcite precipitation model (Barry et al., 2020) at variable temperatures (50, and 192 ℃).

The calculation results of the mixing ratio values of the three endmembers of the geothermal gases in the Yangbajing area are listed in Table 3. The proportion of the carbonate components was 54%–68%, with an average of ∼60%. That of the sediment component ranged from 26% to 43%, with an average of ∼35%. The average ratio of the mantle endpoints was ∼5%. The high ratio of the carbonate and C/S (carbonate/sediments) value in the geothermal gases in the Yangbajing area indicated an obvious heterogeneity of the CO_2 reservoir in the rift area. Moreover, a C/S value>1 indicates that the inorganic carbon contribution is greater than that of organic carbon. In the Yangbajing area, the source of organic carbon might have been some metamorphic–sedimentary rocks, including gneiss and migmatite (Singh et al., 1998, Richards et al., 2005). The primary sources of inorganic carbon were marine carbonate rocks, some of which were exposed along the Yadong–Gulu rift near Yangbajing (Coulon et al., 1986, Kapp et al., 2005). The poor δ¹³C might be related to metamorphic rocks under thermal decomposition by magma. The Nyainqentanglha Mountains in the west of Yangbajing carried a large number of deep granitic gneiss when it was exhumed to shallower depths during the Miocene (Kapp et al., 2005). These metamorphic–sedimentary rocks distributed at depths of 7–13 km (Wu et al., 2007) were heated by magma at a depth of 15–18 km to thermogenic degassing. In addition, Paleozoic sedimentary limestone appears in the Yangbajing area (Zhang et al., 2017a), which may be located under metamorphic–sedimentary rocks. Marine carbonate rocks were constantly metamorphosed and decarbonized as they were heated by high-temperature magma, producing about 60% of the inorganic CO_2 gas, along with mantle-derived CO_2 (∼5%) and metamorphic degassing CO_2 (∼35%) rising into the shallow geothermal system. Newell et al. (2008) specifically discussed the metamorphism and decarbonization of marine carbonate rocks, which are prevalent in the Himalayas and

southern Tibet and can provide a significant amount of metamorphic CO_2 to aquifers (DeCelles et al., 2014, Kapp and DeCelles, 2019).

It should be noted that as geothermal fluids rise to the surface, they usually involve degassing, calcite precipitation, and other phase separation processes. These affect the He–CO_2 characteristics (such as $\delta^{13}C$–CO_2 and $CO_2/^3He$) of hydrothermal fluids (Ray et al., 2009, Barry et al., 2014). The continuous degassing in the local thermal system without deep-source CO_2 replenishment led to the decreased He concentration and the very high $CO_2/^3He$ ratio in the collected gas samples (Ozima and Podosek, 2002). Conversely, degassing of hydrothermal systems at low temperatures (<110 °C) also increases the $\delta^{13}C$ value in the remaining liquid (Mook et al., 1974). This can be seen in the samples with low $CO_2/^3He$ ratios, such as sample ZK4001 (Fig. 12). The samples were affected by calcite precipitation; the isotopic characteristics were consistent with the precipitation curves of calcite at 25 °C–192 °C (Ray et al., 2009, Güleç and Hilton, 2016).

5.4. Deep temperature from the geothermometers

5.4.1. Gas ratio geothermometer

The gas samples in the Yangbajing area fall in the region with R_H = −3.6 to −3.2. This indicates that the oxidation state of the geothermal fluid varies greatly, which may be related to the Ar concentration. Ar is generally associated with shallow water – gas reactions, which inherently depend on the aquifer thickness and upward flux of deep hydrothermal fluids. Mixing with atmospheric Ar also changes the H_2/Ar ratio, thus reducing the estimated temperatures. Previous studies showed that the shallow reservoir of Yangbajing (<400 m) also had mixing of cold water and deep thermal fluid, and mixing with shallow oxygen-rich cold water may have stimulated a secondary oxidation process and thus consumed H_2. This is supported by the oxidation state coefficient in the Yangbajing area is lower than that of the $FeO/FeO_{1.5}$ buffer (R_H = −2.8), which is a common pair in geothermal systems. This suggests that deep fluids were either oxidized during ascent or mixed with shallow oxidizing fluids, which is consistent with the predicted lower reservoir temperatures.

The resulting temperature range is significantly lower than the measured temperature value (329.8 °C) of borehole ZK4002. This may be because the CO_2–CH_4 system had obvious H_2 rebalancing when the geothermal fluid rose to the surface. In addition, the oxidation state of the CO_2–CH_4–H_2 equilibrium system was stronger than that of the original hydrothermal system (R_H = −2.8) (Giggenbach, 1987, Sepúlveda et al., 2007, Cinti et al., 2014). This low R_H value generally considers the gas–liquid interactions that occur at ∼140 – 160 °C. Therefore, it can be inferred that the CO_2–CH_4–H_2 equilibrium system is very sensitive to the rebalancing of H_2 due to the decreased temperature. After considering the CO_2–CH_4–H_2 re-equilibrium system, the temperature calculated by the CH_4–CO_2 system Eq. (3) at R_H = −2.8 is 250 ± 15 °C, which can be considered as an estimation of the deep reservoir

(~2 km, Fig. 3) temperature in the Yangbajing geothermal field and it is consistent with borehole temperature measurement (Guo et al., 2007).

There are kaolinite, muscovite, sulfate and natural sulfur, anhydrite, alunite, and other alteration minerals in the northern part of Yangbajing and calcite (travertine) in the southern part (Dor et al., 1997). The characteristics of the altered minerals show that the Yangbajing area experienced different redox states in history. However, the present geothermal water is slightly alkaline, with low SO_4, Cl-dominated hot water, and calcite (travertine) as the main precipitate. These indicate that the geothermal system of Yangbajing gradually attained a stable chemical equilibrium state.

On the basis of the above analysis, we prefer that the existence of the weak oxidation state in the gas components may be related to the mixing of the geothermal fluid and shallow cold water during migration. Gas composition rebalancing has occurred, which is more reflective of the shallow geothermal reservoir (~500 m, Fig. 3) temperature of 150 ± 15 ℃ (Fig. 4). This result also considered gas composition measurement errors. In addition, this result is consistent with previous research and borehole temperature measurement results (Guo et al., 2007).

5.4.2. Soil CO_2 flux geothermometer

The soil CO_2 flux geothermometer was developed based on the principle of an earlier CO_2 geothermometer (Arnórsson and Gunnlaugsson, 1985) and a large number of CO_2 flux measurement data sets (Harvey et al., 2017). The thermodynamic principle of previous CO_2 geothermometers was that the concentration of CO_2 in high-temperature hydrothermal geothermal systems is controlled by basic water–rock reaction: plagioclase + CO_2 = clay + calcite (Giggenbach, 1981). Empirical geothermometers assume that geothermal reservoir fluids go through adiabatical boiling from the reservoir to the atmosphere. Thus, the CO_2/H_2O ratio in geothermal reservoirs can be obtained by measuring those in surface fumaroles. At a certain temperature, deep geothermal water boiling at atmospheric pressure is accompanied by a certain mass fraction of steam separation, enabling the prediction of a reservoir's CO_2/H_2O ratio from fumaroles. However, nonadiabatic heat transfer to the surface, such as secondary boiling or steam condensation in fumaroles, makes geothermometer less suitable. In addition, pulsed degassing CO_2 from magma may overwhelm the mineral buffering capacity of overlying geothermal reservoirs, resulting in unbalanced, physically controlled reservoir CO_2 concentrations and higher soil CO_2 flux.

Following the frameworks of Harvey et al. (2017), we used the soil CO_2 flux and soil temperature in the Yangbajing area to derive the reservoir temperature. Fig. 5 shows that the reservoir temperatures obtained using the heat flux formula of Hochstein and Bromley's (2005) are lower than those obtained using Seward et al.'s (2018) formula. This difference may be explained by Seward et al.'s (2018) improvement of Hochstein and Bromley's (2005) soil heat flux formula. The new formula derived from more data and thus could better reflect the characteristics of concentrated heat release in geothermal anomaly areas. Therefore, the estimated heat reservoir temperatures obtained using the new formula were generally slightly higher. However, no matter which soil heat

flux formula was used, the estimated mean temperatures were not significantly different ($\sim$10 ° C) in the north and south geothermal areas or the whole Yangbajing geothermal area, especially for the high-temperature geothermal area northwest of Yangbajing. Therefore, the results based on Seward et al.'s (2018) formula prevail in the following discussion.

It may be inferred that there is a distinct characteristic display in the northwestern geothermal area of the Yangbajing geothermal field. As a geothermal fluid seepage zone, it has a high reservoir temperature (about 280 ℃), whereas the reservoir temperature of the entire Yangbajing geothermal field is $\sim$257 ° C. This result is very close to the measured temperature of 252 ° C from borehole ZK4001.

The value of the reservoir temperature is consistent with the soil CO_2 flux (Zhang, 2015), indicating that CO_2 flux is controlled by H_2O flux. According to the calculation process (Table S2), the CO_2 flux greatly varies, indicating a very heterogeneous shallow CO_2 channel or deep fractures or highly permeable soil cover in the concentrated area. The H_2O flux is converted from an empirical relationship of the soil temperature, and the accuracy of calorimetry measurements has been validated in the Taupo Volcanic Zone of New Zealand (Rissmann et al., 2012, Bloomberg et al., 2014). However, the regression equation for determining the boiling point depth was measured in the Taupo Volcanic Zone in summer with an air temperature of 20 ℃. In this paper, the soil CO_2 in Yangbajing was also measured in summer, but the average air temperature in the plateau area was slightly lower than that in the Taupo Volcanic Zone. From the estimation results of the reservoir temperature, such temperature difference may introduce a relatively large error, but it is impossible to draw a conclusion at present. If a more accurate regression equation is to be obtained, conducting soil temperature measurements at multiple plateau geothermal areas will be necessary for the future to correct the boiling point depth.

Our reservoir temperature estimation results show that the reservoir temperature is consistent with some previous research results (Zhao et al., 1998, Guo et al., 2007), albeit in a broader range (Fig. 13). This range could be because of subsurface differences or various measurement errors. First, an important factor is the heterogeneity of the permeability of the cover layer in the shallow part of the geothermal area that prevents gas from escaping to the atmosphere. For example, huge variability in the CO_2 flux occurs when the ground is altered (Chiodini et al., 1996), and the nonuniform permeability caused by such alteration has been demonstrated in Wairakei and Reporoa, New Zealand (Bloomberg et al., 2014). Therefore, the heterogeneous permeability of the shallow crust can significantly affect the flux of CO_2 and H_2O vapor, leading to the condensation of water vapor at the bottom of the low-permeability layer. In addition, in some areas with high soil moisture, the high water content slows the discharge of CO_2 into the atmosphere, resulting in underestimated reservoir temperatures. Moreover, in some places where fumaroles exist, underground CO_2 rapidly reaches the atmosphere via advective methods. Such point-source CO_2 excretion significantly increases CO_2 and H_2O fluxes, resulting in abnormally high reservoir temperature values. However, these are examples of extreme cases and rarely occur. Generally, variations in the reservoir temperature estimated using the CO_2 flux are mainly caused by differences in the water vapor and CO_2 fluxes caused by spatial differences in permeability.
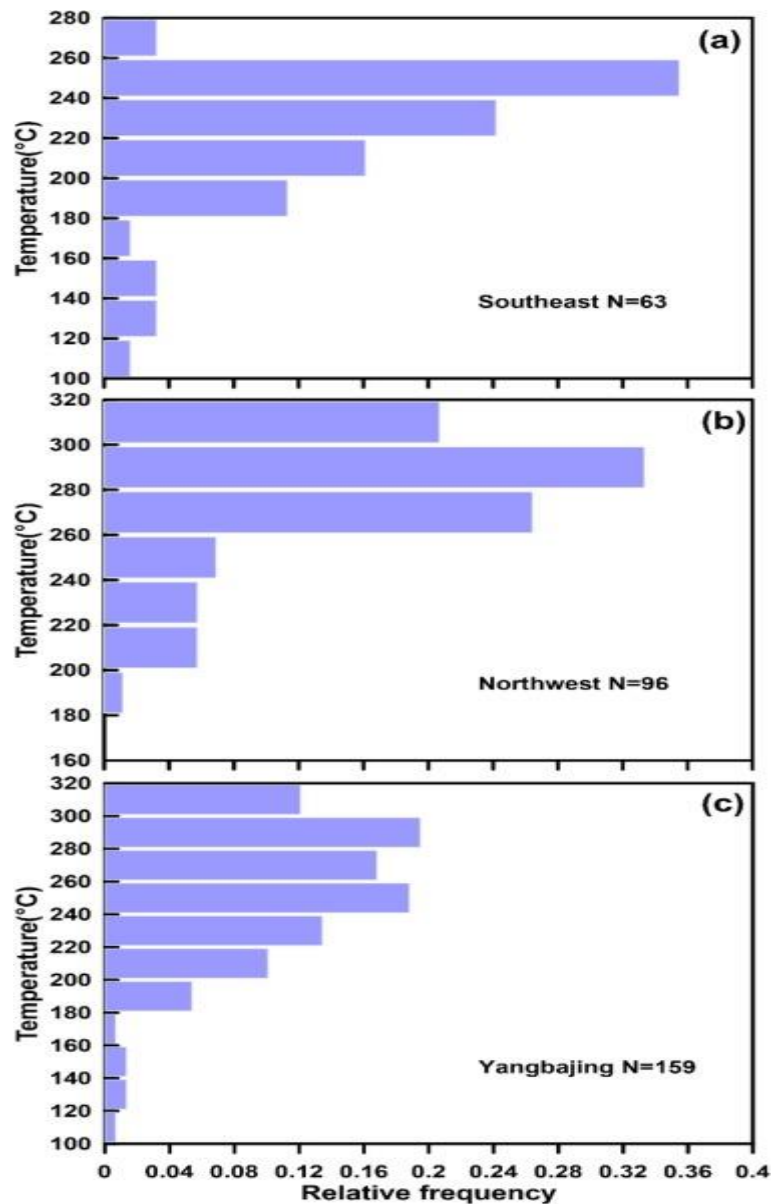
Fig 13. Histogram of reservoir temperature results from soil CO_2 flux geothermometer.

In addition, according to the genesis model of the Yangbajing geothermal field (Fig. 3), the geothermal system is located in a rift valley. Therefore, it has multiple layers of thermal reservoirs at different depths. Those with temperature estimates over 300 ℃ may represent deeper reservoir (may be >5 km) temperatures, consistent with the fact that most of the CO_2 gas came from deep thermogenic decarbonization. Moreover, in their study on the factors influencing soil CO_2 flux measurements, Fairley and Hinds (2004) reported that the deep fractures in the rift zone contributed to the direct arrival of deep CO_2 to the surface (Lewicki et al., 2003, Hunt et al., 2017). Such deep-source CO_2 likely represents the deep temperature information of the rift zone. Considering that the extremely high CO_2 flux was affected by some extreme conditions, we selected the 90% quantile representing the deep reservoir (over 5 km) temperature (Fig. 13) of about 327 ℃. This temperature value may represent the upper limit of the reservoir temperature in the Yangbajing area. Further, the geothermal gradient of 4 ℃/100 m in this area (Kang et al., 1985) indicates that the circulation depth of the geothermal fluid has reached ~8 km, which is

consistent with that of Gonghe Basin, north of the Tibetan Plateau (Pan et al., 2021). However, this depth exceeds the 2–6-km depths of typical supercritical fluids, and ~320 ℃ is far lower than the supercritical temperature of pure water. Therefore, we prefer that there is no condition from reservoir temperature of the existence of supercritical geothermal fluids in the Yangbajing geothermal field.

5.4.3. Noble gas geothermometer

Noble gas geothermometer has attracted great attention because of its insensitivity to secondary processes and chemical re-reactions (Mazor and Truesdell, 1984). However, isotopic fractionation due to boiling and phase separation also results in defects (Mazor et al., 1990, Pinti et al., 2017). Thus, the water–gas equilibrium of atmosphere-derived noble gas (ANG) isotope (^{20}Ne, ^{36}Ar, ^{84}Kr) abundance in geothermal waters controlled by temperature is developed as a new geothermometer (Byrne et al., 2021).

According to the He and C isotope analysis, the gas in Yangbajing was mixed with a certain proportion of atmosphere-derived gas. This was mainly due to the influence of deep geothermal fluids that reach shallow depths and mix with cold water. However, the ^{4}He/^{20}Ne ratio of one sample showed obvious atmospheric pollution due to operational problems during the sampling process, which was not considered in the estimation of the reservoir temperature. In addition, the CO_2/^{3}He relationship showed that the mantle-derived part of the gas samples comprised less than 3% of the total samples. Therefore, we can consider that the noble gas isotopes collected in the geothermal fluid have atmospheric isotope signatures, which entered the ground after the infiltrated meteoric water and air reached dissolution equilibrium. The noble gas isotope component of the ASW is an endmember.

Fig. 6 shows the relationships of the ^{20}Ne, ^{84}Kr, and ^{36}Ar abundances, which fit well with the estimated fractionation lines at temperatures between 200 ℃ and 350 ℃. Notably, even if the air endmember is also shown on this curve, if the noble gas is contaminated with some air, the data points plot close to the air side, resulting in an underestimation of geothermal reservoir temperatures, although the data points are still close to the mixing curve. In addition, when a high proportion of vapor (X_v) is present, the abundance of ANG is significantly reduced, and the data points are shifted toward the vapor phase. This results in overestimated reservoir temperatures. Therefore, a temperature estimation method considering the air mixing ratio should be introduced.

Fig. 7 shows that the extra amount of air mixed into the gas samples is caused by either the sampling process or the degassing process, which increases the ANG abundance and leads to underestimated reservoir temperatures. According to the relationship of ^{84}Kr/^{36}Ar and ^{20}Ne/^{36}Ar vs. 1/^{36}Ar (Fig. 7), air mixing causes adverse effects on the estimation of reservoir temperatures. The samples show apparent deviations from the vapor phase separation line and are close to the air end element. However, this correction might be imperfect because a small fraction of the gas isotopes came from the mantle. Our correction mainly considered only the effects of atmospheric mixing. Nonetheless, the gas source shows that the influence of mantle gas mixing of less than 3% on the estimation of reservoir temperatures can be ignored. Based on results of this new type of geothermometer, the temperature of the

geothermal reservoir in Yangbajing is around 250 ± 10 ℃ (Fig. 7), which is determined through the comparative analysis of the single noble gases and multiple noble gas mixtures.

It is important to note that conventional gas geothermometers primarily consider temperatures at the last stage of gas–rock equilibria. However, noble gas geothermometer record temperatures at which gases and liquids coexist in reservoirs at phase separation equilibria. Therefore, we must not expect that the reservoir temperatures obtained using multiple methods will be identical. However, different geothermometers can reflect the evolution of reservoir temperatures at different stages. Generally, the reservoir temperatures obtained by noble gas geothermometers are consistent and acceptable. The differences in the results of various geothermometers indicate that each geothermometer has its applicable conditions and complexities. However, the obvious advantage of noble gas geothermometers is that the chemical reactions during the ascent of geothermal fluids can be ignored.

5.5. Conceptual model of fluids in the Yangbajing geothermal field

The gas volatiles in the geothermal water are the vectors of mass and energy transfer from the deep geothermal system to the surface, reflecting the heat source properties and the origin of the parent fluid. The relationship between the He and C isotopes of the geothermal gases reveals that the Yadong–Gulu Rift (YGR) can be divided into the southern, middle, and northern sections (Zhang et al., 2021). The southern segment is dominated by the decarbonization of Himalayan metamorphic rocks. The middle segment is dominated by the decarbonization of marine carbonate rocks and metamorphic sediments. The northern segment is dominated by the decarbonization limestone resulting from asthenosphere upwelling (Zhang et al., 2021). Geophysical observations also confirm that mantle effects are absent in the Himalayan accretion wedge; instead, mantle effects on the extensional rift appear in the north part of the Lhasa block (Shi et al., 2020). Yangbajing is located south of middle YGR, southeast of Nyainqentanglha Mountains, which formed during the Miocene when anatexis granite was exhumed to the surface (Kapp et al., 2005). The depth of the melt in the Yangbajing area is 15–18 km, and the mechanism of its formation is still controversial (Fig. 14b). Although it has been proposed that asthenosphere upwelling is the dominant heat source that caused melting in the middle crust, the most typical insufficiency of this proposition is that the samples are all pre-Miocene (Liu et al., 2017, Tian et al., 2017). There is still no direct evidence for the correlation between middle-crust melting and the mantle after the Miocene (Xie et al., 2021). However, it has been established that the melt is independent of mantle-derived magma. The main reason is that eclogitization occurred in the subduction front of the Indian continent, which halted the further upwelling of deep-mantle magma (Tian et al., 2020). Searle et al. (2010) suggested that the middle-crust melt resulted from thermal relaxation and radiogenic heat due to the thickening crust (∼80 km). The three-dimensional thermomechanical coupling numerical simulation of Chen et al. (2019) showed that radioactive heat generation played a dominant role in the melting of the middle crust, with shear deformation heat playing a secondary role. The low proportion of mantle-derived gases in this paper also indicated the limited contribution of mantle heat to the current melts. Therefore, asthenosphere upwelling had almost no relation and contribution to the present melt at the Yangbajing area. The present melt in

the middle crust resulted from anatexis under the coupling of radioactive heat generation and shear deformation heat (Nábělek et al., 2009, Searle et al., 2010, Tian et al., 2020).
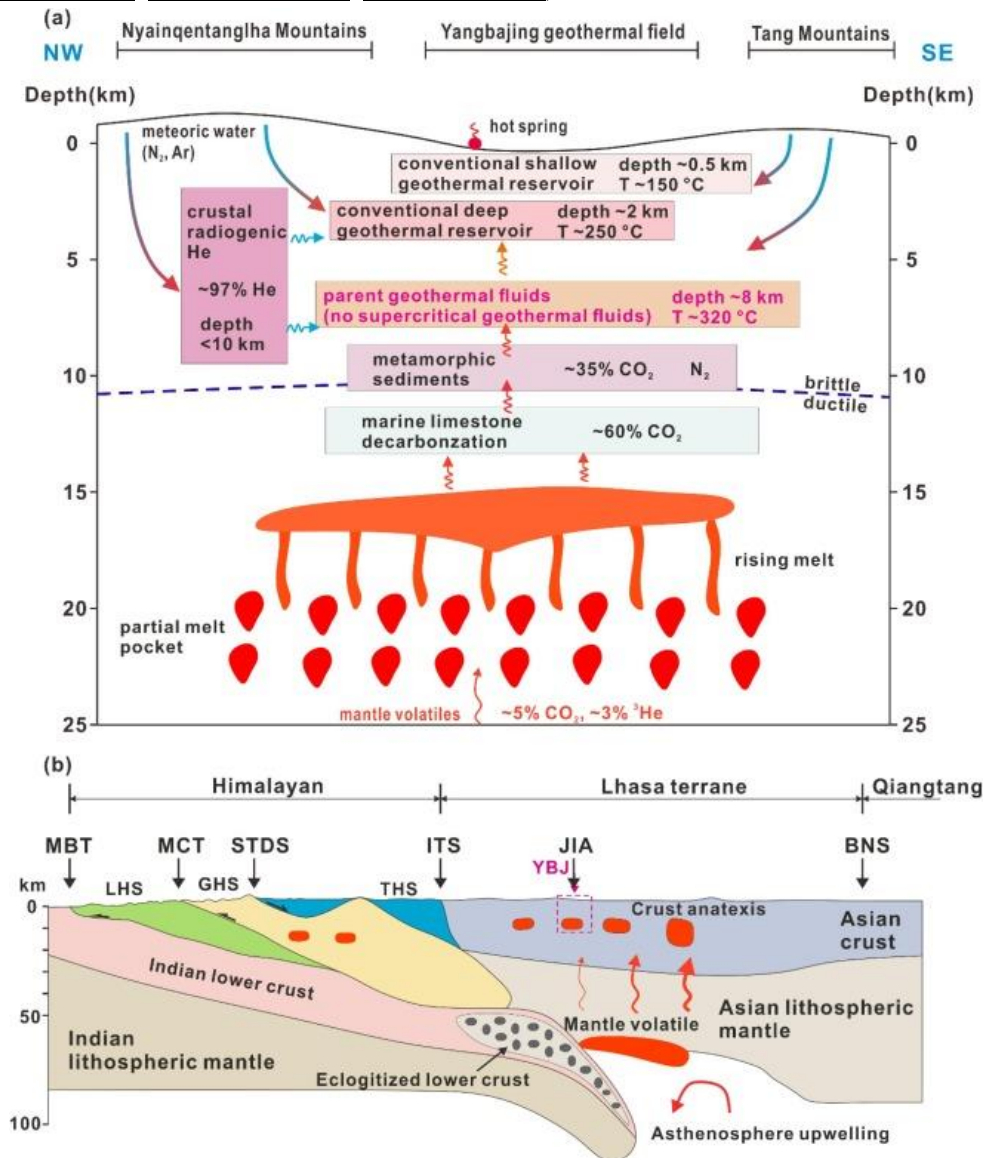

Fig. 14. The conceptual model of the evolution and migration of gases in the Yangbajing geothermal field. Abbreviations in (b): MBT, main boundary thrust; MCT, main central thrust; STDS, southern Tibet detachment system; ITS, Indus-Tsangpo suture; BNS, Bangong-Nujiang suture; LHS, Lesser Himalayan sequence; GHS, Greater Himalayan sequence; THS, Tethyan Himalayan sequence; JIA, Junction belt between the Indian and Asian continents; YBJ, Yangbajing geothermal field.

On the basis of the systematic analysis of geothermal gases in the Yangbajing geothermal field, combined with previous seismic and magnetotelluric detection results from the area, the evolution model of the geothermal gases in Yangbajing can be summarized as follows. As the Indo-Eurasian collision orogeny began about 60 Ma, a large area of the Tethys Ocean Basin was closed, and sedimentary strata were buried at depth (Hu et al., 2016). This was followed by a north–south compression, which formed a series of north–south trending rift graben systems in the Qinghai–Tibet Plateau. These provided preponderant channels for deep materials and energy to rise to the surface (Su et al., 2020). Yangbajing is the most representative rift basin in the Qinghai–Tibet Plateau. A localized melting

zone with a depth of 15–18 km in this area is speculated as a vital heat source (Guo et al., 2007) that provides energy and gas materials to the geothermal system. Very low percentages (<5%) of mantle-derived volatiles (CO_2 and ^3He) gradually migrated upward to about 10–12 km at the brittle–ductile transition (BDT) zone (Góbelin et al., 2017). At depths around the BDT, CO_2 gas from the thermogenic decarbonization of carbonate rocks and metamorphic sediments at about 400 ℃ (Ferry, 1992) and other gases (e.g., N_2) mixed with the rising magmatic volatiles (Molnar, 2020). These mixed gases continued to migrate upward and reached the geothermal reservoir at a depth of ∼8 km. The estimated reservoir temperature based on the soil CO_2 geothermometer was ∼320 ° C. At this temperature, the geothermal fluids mixed with the infiltrated atmospheric precipitation and radiogenic helium to form the parent fluids of the geothermal field, which are mainly concentrated in the granite strata northwest of Yangbajing. These mixed fluids then migrated to shallower depths along the deep fault in front of the Nyainqentanglha Mountains. Then they were mixed with shallow cold water and atmospheric gases along their journey. The mixed fluids reached shallow Quaternary depths (∼500 m) and then migrated laterally to the southeast of the geothermal field (Fig. 3) to form the shallow geothermal reservoir in Yangbajing (Guo et al., 2007). The evolution mode of the geothermal fluids of the Yangbajing geothermal area is shown in Fig. 14.

Our fluid evolution model is not inconsistent with previous results (Guo et al., 2007, Wang et al., 2018). However, these earlier studies focused on the characteristics and evolution of conventional geothermal fluids in shallow reservoirs (<3 km) at Yangbajing. In this paper, the geological controls of the formation of deeper (∼8 km) geothermal fluids and the possibility of the existence of supercritical geothermal fluids were analyzed by exploring the characteristics of gases combined with geophysics, geochemistry, and recent achievements. The Yangbajing geothermal system is a product of orogeny; thus, its formation and evolution are closely related to tectonic processes (Alt-Epping et al., 2021). The melts discussed in this study provided favorable conditions for the formation of a high-temperature geothermal system and further thermogenic decarbonization to produce CO_2-bearing geothermal fluids in shallow areas.

5.6. Implications for the supercritical geothermal fluids in Yangbajing

5.6.1. Comparison of the He–C isotopes with those of other supercritical geothermal fields

Ultra-high-temperature recoverable geothermal energy sources have always been the goal of geothermal scientists. They are particularly concerned about those close to magma bodies whose temperatures exceed the supercritical state when detecting hydrothermal fluids deeper than those of conventional geothermal reservoirs (Scott et al., 2016). Since Iceland began exploring supercritical geothermal fluids in 2001 (i.e., the IDDP Project) (Elders et al., 2014), over 10 places with potential supercritical geothermal fluids have been found around the world (Reinsch et al., 2017). By comparing their isotopic characteristics with those of the He and C isotopes of the gases in Yangbajing, we hope to find evidence of no supercritical geothermal fluids in the Yangbajing area. In this paper, water and gas chemistry data from Yangbajing were studied intermittently over 20 years. From the earlier analyses,

we can infer that the Yangbajing geothermal field showed relatively stable $CO_2/^3He$ and R/R_a values during its evolution for more than 20 years. The helium isotope ratios were generally less than 0.2 Ra (Fig. 10). Although the degassing process may have affected and changed the $\delta^{13}C$ value, $CO_2/^3He$ did not differ by an order of magnitude over 20 years (Fig. 12), indicating a stable deep heat source and a volatile source at Yangbajing.

We sorted out the relationships between the He and C isotopes of the typical supercritical geothermal systems worldwide in Fig. 15: Yellowstone, USA (Bergfeld et al., 2014, Lowenstern et al., 2015); Krafla, Nesjavellir, and Reykjanes, Iceland (Füri et al., 2010, Barry et al., 2014); Los Humeros (Pinti et al., 2021); The Geysers (Lowenstern et al., 1999, Bergfeld et al., 2001, Moore et al., 2001); Menengai, Kenya rifts (Darling et al., 1995, Lee et al., 2017); and Laderello (Gherardi et al., 2005). The plotted endmembers included MORB, oceanic island basalt (OIB), continental lithospheric mantle (CLM), and arcs (worldwide arc average). The $CO_2/^3He$ and R/R_a values for MORB were $0.2–3 \times 10^9$ (Marty and Zimmermann, 1999) and 6.5–9.5 (Graham 2002), respectively. Meanwhile, those for OIB were not particularly uniform around $2–20 \times 10^9$ and 9–30, respectively (Graham 2002). The $CO_2/^3He$ and R/R_a values for CLM varied from 10^9 to 10^{11} (Day and Hilton, 2020) and 2–7.8, respectively (Dodson et al., 1998). Fig. 15 shows that the R/R_a vs. $CO_2/^3He$ plots for all the typical supercritical geothermal systems fall in the region directly related to magma. This is because, for instance, Iceland is primarily associated with OIB, Yellowstone with a mid-ocean ridge or the continental asthenosphere, Los Humeros with island arc magma, and Kenya rift with CLM. In contrast, Yangbajing has no relation with mantle-derived magma. Further, the He–C isotope characteristics of the Yangbajing area indicate that there may be no supercritical geothermal fluids therein. Moreover, we can infer that the formation of supercritical geothermal fluids is closely related to magma chambers. Thus, the magma chamber characteristics of Yangbajing and other typical supercritical geothermal systems are further compared.
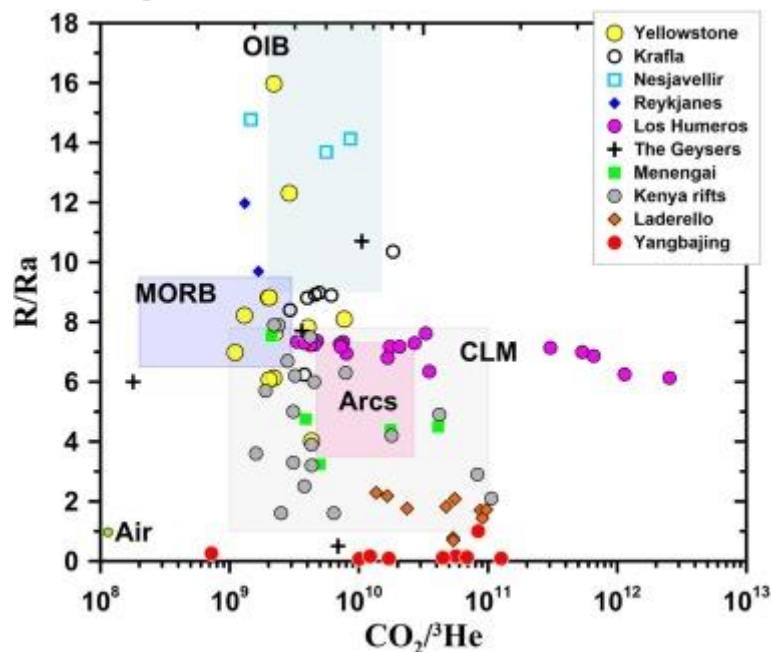

Fig. 15. He–C isotope characteristics of Yangbajing and other supercritical geothermal fields around the world. Data source: Yellowstone (Bergfeld et al., 2014, Lowenstern et al., 2015); Krafla, Nesjavellir, and

Reykjanes (Barry et al., 2014, Füri et al., 2010); Los Humeros (Pinti et al., 2021); The Geysers (Moore et al., 2001, Bergfeld et al., 2001, Lowenstern et al., 1999); Menengai, Kenya rifts (Lee et al., 2017, Darling et al., 1995); and Larderello (Gherardi et al., 2005).

5.6.2. Comparison of the Yangbajing magma chamber with those of other supercritical geothermal fields

The characteristics, burial depth, and volume of magma are all crucial factors for the formation of supercritical geothermal systems. In this study, we collected the characteristics of the magma chambers of Yangbajing and the world's supercritical geothermal systems (Table 4). We then compared and analyzed the mechanisms of the nonexistence of a supercritical geothermal system at Yangbajing.

Table 4. The magma type, burial depth, magma volume, and melt temperature of several supercritical geothermal fields worldwide.

Geothermal field	Magma type	Buried depth (km)	Magma volume (km^3)	Melt temperature (°C)	References
Yangbajing	Granitic magma	15–18	500–600	650–700	Zhao et al., 1998, Hacker et al., 2014, Xie et al., 2021
The Geysers	Andesitic magma	7	>3000	900–1000	Dalrymple et al., 1999, Hurwitz and Lowenstern, 2014, Peacock et al., 2020
Kakkonda	Andesitic magma	4–5	500	900–1000	Muraoka et al., 1998, Amanda et al., 2019
Menengai	Andesitic magma	4–5	200	900–1000	Kanda et al., 2019
Krafla	Basaltic magma	–3	1000	1100–1200	Heimisson et al., 2015, Kim et al., 2017, Kim et al., 2020
Yellowstone	Basaltic magma	4–5	10,000	1100–1200	Farrell et al., 2014, Huang et al., 2015
Campi Flegrei	Basaltic magma	3	6000	1100–1200	Mangiacapra et al., 2008, Marturano et al., 2018; Townsend and Huber, 2020
Los Humeros	Basaltic magma	5–8	1400	1100–1200	Verma and Gómez-Arias, 2013, Lucci et al., 2020
Reykjanes	Basaltic magma	2.5	>2000	1200–1300	Chen, 2003, Scott, 2021
Nesjavellir	Basaltic magma	4.5	3500	1100–1200	Árnason et al., 2010, Gasperikova et al., 2015
Salton sea	Rhyolitic magma	4–12	500–1000	700–800	Brothers et al., 2009, Karakas et al., 2017

Geothermal field	Magma type	Buried depth (km)	Magma volume (km^3)	Melt temperature (℃)	References
Larderello	Granitic magma	3–8	1500–2000	700	Vanorio et al., 2004, Bertini et al., 2006, de Franco et al., 2019, Bagagli et al., 2020

The formation of supercritical geothermal systems is closely related to the tectonic background of geothermal fields. According to various geological and geophysical data, no Quaternary volcanic activity has been found in the Yangbajing area up to now (Zhao et al., 2001, Teng et al., 2019). Moreover, the type of heat source in the Yangbajing geothermal field was previously controversial (Tong and Zhang, 1981, Hochstein and Regenauer-Lieb, 1998). However, as discussed in section 5.5, the heat energy generated from shearing deformation and radioactive elements during collisions caused the anatexis of the sedimentary rocks in Yangbajing, forming a granitic magma with a minimum melting temperature of 650 ℃ (Makovsky and Klemperer, 1999, Chen et al., 2018). This discontinuous, distributed melt is deduced as the heat source of geothermal systems in plateaus such as Yangbajing (Hetényi et al., 2011), with a maximum single volume of 500–600 km^3 (Hacker et al., 2014). This results in the evident surface thermal manifestations and high-temperature geothermal reservoirs within the geothermal area. However, the essential nature of magma chambers is significantly different in supercritical geothermal systems related to active volcanic regions and hot spots such as Krafla in Iceland; Larderello in Italy; The Geyser, Salton Sea, and Hawaii in the United States; Menengai in Kenya; Los Humeros in Mexico; and Kakkonda in Japan (Reinsch et al., 2017). In these supercritical geothermal areas, the magma sources are pre-basic magma, such as andesitic magma (melting temperature 900 ℃–1000 ℃) (Fedotov, 1981) or basaltic magma (melting temperature 1100 ℃–1200 ℃) (Delaney and Pollard, 1982). These basic magma melts can provide more heat energy to the shallow crust. Therefore, the different nature of the deep magma chamber in the Yangbajing geothermal field may be the first reason why there are no supercritical geothermal fluids therein.

A very simple truth is that the less the distance between the heat source and the reservoir, the easier the formation of a supercritical geothermal system. According to the results of multimethod geophysical surveys in the Qinghai–Tibet Plateau, the emplacement depth of the magma chamber in the Yangbajing area is about 15–18 km (Hacker et al., 2014), which is indeed deep enough for most high-temperature geothermal systems. Compared with the emplacement depths of the magma chambers of other supercritical geothermal systems worldwide, the emplacement depth in the Yangbajing area is much deeper. In contrast, those of other systems are around 7 km (the Geysers, USA) (Dalrymple et al., 1999), 4–5 km (Kakkonda, Japan, and Menengai, Kenya, among others) (Muraoka et al., 1998, Kanda et al., 2019), and even ~3 km (Krafla, Iceland) (Kim et al., 2020). Such deep heat source in Yangbajing raises another problem: the permeability of the surrounding rock. Scott et al. (2015) specifically studied the geological controls for the formation of supercritical geothermal systems, and one critical parameter is permeability. This is because high permeability ($>10^{-15}$ m^2) is more conducive to geothermal

fluid migration and rapid heat transfer. Such permeability occurs at depths less than that of the BDT zone (4–6 km) in many geological conditions (Watanabe et al., 2017, Jolie et al., 2021). Another important feature for supercritical geothermal fluid formation is that supercritical geothermal fluids occur almost within 1 km above the magma chamber. Such area results from the combined heat transfer efficiency and permeability (Scott et al., 2015), and this requires a shallow emplacement depth of the magma chamber. The depth of the BDT zone in the Yangbajing area is about 11 km (Weller et al., 2016). On the basis of the distance between the magma chamber and the BDT, the geological conditions in the Yangbajing geothermal field might be unfavorable for the formation of a supercritical geothermal system because of Yangbajing's deeply emplaced magma chamber.

The magma chamber in the Yangbajing geothermal field formed from the partial melting of sedimentary rocks in the crust, and its size might be too small for such a formation mechanism. According to the volume of the low-velocity area beneath the Yangbajing geothermal field, the maximum single volume does not exceed 2000 km^3 (Hacker et al., 2014, Het ényi et al., 2011). On the basis of the maximum melt ratio of 30% in southern Tibet, the current largest volume of the magma chamber is less than 600 km^3 (Chen et al., 2018). This scale is an order of magnitude different from those of other supercritical geothermal fields worldwide. By systematically comparing the volumes of the magma chambers beneath the discovered supercritical geothermal systems (Table 4), we can see that their volumes are generally greater than 1000 km^3. Even so, those systems with volumes of only a few hundred cubic kilometers also have another characteristic, that is, their burial depths are very shallow (∼3 km) (e.g., Krafla). Therefore, the volume of the magma chamber beneath the Yangbajing geothermal field also negates the existence of supercritical geothermal fluids therein.

6. Conclusions

This paper presented a systematic analysis of the components and isotopes of the geothermal fluids in the Yangbajing geothermal field. Using multi-gas geothermometers, we estimated the reservoir temperatures of the Yangbajing geothermal field, and relatively acceptable results were obtained. Moreover, we determined that there are no supercritical geothermal fluids in the Yangbajing area after comparing Yangbajing's geothermal and geological characteristics with those of other supercritical geothermal systems worldwide. The specific conclusions are as follows:

The main component of the geothermal gases in the Yangbajing geothermal field was CO_2, with a volume percentage of more than 70%. N_2 was mainly derived from mixing with gases from metamorphic degassing and the atmosphere. The multi-isotopic relationship of CO_2 and He revealed that the high CO_2 content of the samples is related to the thermogenic decarbonatization of marine carbonates and metamorphic sediments. He mainly originated from radioactive decay in the crust, whereas the magma-derived volatiles comprised less than 3% of the total samples.

Using the CO_2 –CH_4–H_2 gas thermometer, soil CO_2 flux geothermometer, and noble gas geothermometer, we constrained the reservoir temperatures of the Yangbajing geothermal field. We determined at least three reservoirs.

The third reservoir was the source of the parent geothermal fluid, with temperatures of ~320 ° C and a depth of ~8 km. The second reservoir had a temperature of ~250 $\pm$ 10 ° C, whereas the first reservoir had a temperature of 150 $\pm$ 15 ° C.

Comparing the geochemical (He–C isotope) and geological (magma chamber) characteristics of supercritical geothermal fields, we inferred that the Yangbajing geothermal field could not host supercritical geothermal fluids with less mantle-derived volatiles (CO_2 < 5% and He < 3%) and its fairly deep-seated, small-volume granitic magma chamber.

CRediT authorship contribution statement

Yingchun Wang: Conceptualization, Formal analysis, Investigation, Methodology, Writing – original draft, Writing – review & editing. Liang Li: Investigation, Writing – review & editing. Huaguo Wen: Conceptualization, Data curation, Project administration, Funding acquisition, Writing – review & editing. Yinlei Hao: Data curation, Methodology, Writing – review & editing.

Declaration of Competing Interest

The authors declare that they have no known competing financial interests or personal relationships that could have appeared to influence the work reported in this paper.